STRUCTURAL CHEMISTRY

ISSN 2053-2296

Geometric isomers of dichloridoiron(III) complexes of CTMC (5,7,12,14-tetramethyl-1,4,8,11-tetraazacyclotetradecane)

Stephanie S. DeLancey, Reese A. Clendening,* Matthias Zeller and Tong Ren

Department of Chemistry, Purdue University, 560 Oval Dr., W. Lafayette, IN 47907-2084, USA. *Correspondence e-mail: rclende@purdue.edu

Received 18 July 2022
Accepted 24 August 2022

Edited by T.-B. Lu, Sun Yat-Sen University, People's Republic of China

Keywords: stereoisomerism; iron(III) macrocyclic complexes; geometric complex control; crystal structure; tetraazacyclotetradecane; CTMC.

CCDC references: 2203222; 2203221; 2203220

Supporting information: this article has supporting information at journals.iucr.org/c

Both *trans* and *cis* iron–CTMC complexes, namely, *trans*-dichlorido[(5*SR*,7*RS*,12*RS*,14*SR*)-5,7,12,14-tetramethyl-1,4,8,11-tetraazacyclotetradecane]iron(III) tetrachloridoferrate, $[Fe(C_{14}H_{32}N_4)Cl_2][FeCl_4]$ (**1a**), the analogous chloride methanol monosolvate, $[Fe(C_{14}H_{32}N_4)Cl_2]Cl{\cdot}CH_3OH$ (**1b**), and *cis*-dichlorido[(5*SR*,7*RS*,12*SR*,14*RS*)-5,7,12,14-tetramethyl-1,4,8,11-tetraazacyclotetradecane]iron(III) chloride, $[Fe(C_{14}H_{32}N_4)Cl_2]Cl$ (**2**), were successfully synthesized and structurally characterized using X-ray diffraction. The coordination geometry of the macrocycle is dependent on the stereoisomerism of CTMC. The packing of these complexes appears to be strongly influenced by extensive hydrogen-bonding interactions, which are in turn determined by the nature of the counter-anions (**1a** *versus* **1b**) and/or the coordination geometry of the macrocycle (**1a/1b** *versus* **2**). These observations are extended to related ferric *cis*- and *trans*-dichloro macrocyclic complexes.

1. Introduction

Macrocyclic complexes of transition metals, due to the inherent stability imparted by the macrocyclic effect (Constable, 1999), as well as to the ability to tune the number and position of open coordination sites, have often served as model complexes for the study of a number of chemical phenomena. For example, simple tetraazamacrocycles containing iron have been used to investigate aspects of nitrogen fixation (Meyer *et al.*, 1999), nonheme oxoiron (Prakash *et al.*, 2015; Rohde *et al.*, 2003), CO_2 reduction (Straub & Vöhringer, 2021), and water oxidation catalysis (Kottrup & Hetterscheid, 2016). Importantly, the macrocycle may often adopt either a folded or planar coordination geometry, leaving either *cis*- or *trans*-open coordination sites, respectively. This geometry can dramatically influence the reactivity of the resulting complexes (Kottrup & Hetterscheid, 2016; Meyer *et al.*, 1999).

Our group has studied iron–alkynyl complexes supported by cyclam (1,4,8,11-tetraazacyclotetradecane) (Cao *et al.*, 2012), HMC (5,5,7,12,12,14-hexamethyl-1,4,8,11-tetraazacyclotetradecane) (Clendening *et al.*, 2022), and an HMC-derived tetraimine complex (HMTI = 5,5,7,12,12,14-hexamethyl-1,4,8,11-tetraazacyclotetradeca-1,3,8,10-tetraene) (Clendening & Ren, 2022) as models for potential molecular wires. The macrocycle has been shown to strongly affect the properties of these complexes, even tuning the metal–alkynyl bonding. Although Cr^{III}–alkynyl complexes with the macrocycle in both folded and planar conformations have been characterized (Tyler *et al.*, 2016), iron–alkynyl complexes were only isolated with planar macrocycles, even when starting

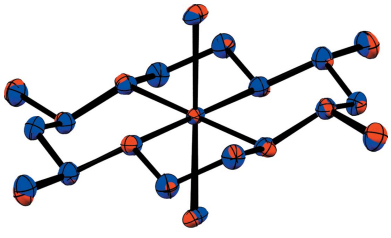

from a *cis*-Fe^{III}(cyclam) complex. Seeking to expand our library of compounds, we have recently turned to the investigation of Fe(CTMC) complexes (CTMC = 5,7,12,14-tetramethyl-1,4,8,11-tetraazacyclotetradecane). Nickel complexes of CTMC (and other macrocycles; Wang *et al.*, 2019) have received considerable attention, most recently as efficient carbon dioxide reduction catalysts (Mash *et al.*, 2019), but no iron complexes of CTMC have been reported previously to our knowledge.

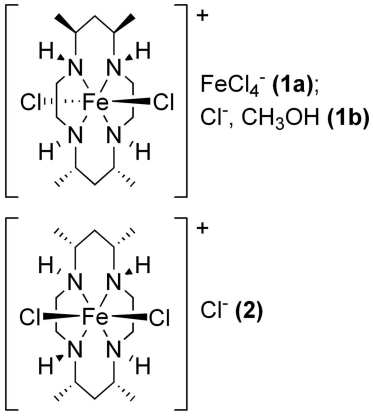

Scheme 1

Although CTMC is known to form as a mixture of stereoisomers, the vast majority of structures contain only isomer **A** [(5*SR*,7*RS*,12*SR*,14*RS*)-5,7,12,14-tetramethyl-1,4,8,11-tetraazacyclotetradecane; Fig. 1]. The structure of the free ligand has been determined, which contained **A** and **B** [Fig. 1; **B** = (5*SR*,7*RS*,12*SR*,14*RS*)-5,7,12,14-tetramethyl-1,4,8,11-tetraazacyclotetradecane] (Tahirov *et al.*, 1995*a*). Finally, the structure of an Ni^{II}(CTMC) complex has been reported containing a third stereoisomer, **C** [(5*SR*,7*RS*,12*RS*,14*RS*)-5,7,12,14-tetramethyl-1,4,8,11-tetraazacyclotetradecane] (Tahirov *et al.*, 1995*b*). Notably, all the structures of metal-ion complexes of CTMC reported to date contain a planar macrocycle.

Here we report the first examples of iron–CTMC complexes and their crystallographically determined structures, namely, *trans*-dichlorido[(5*SR*,7*RS*,12*RS*,14*SR*)-5,7,12,14-tetramethyl-1,4,8,11-tetraazacyclotetradecane]iron(III) tetrachloridoferrate (**1a**), the analogous chloride methanol monosolvate (**1b**), and *cis*-dichlorido[(5*SR*,7*RS*,12*SR*,14*RS*)-5,7,12,14-tetramethyl-1,4,8,11-tetraazacyclotetradecane)iron(III) chloride (**2**). While **1a** and **1b** exhibit the common stereoisomer **A** with a planar macrocyclic conformation, **2** represents the first structurally characterized metal CTMC complex both with stereoisomer **B** and with a folded macrocycle conformation (Fig. 1). Thus, the stereoisomer of the macrocycle appears to control the coordination isomer of the resulting metal complex. Given the importance of macrocycle coordination geometry on the properties of the resultant complex, and the extensive literature on CTMC species, we describe here the structural variations among these species, specifically addressing the differences between the folded (*cis*-dichloro complex) and planar (*trans*-dichloro complexes) coordination motifs. As will be established below, the number and stereochemistry of the macrocyclic substituents can dramatically alter the iron–macrocycle bonding interactions. This work thus serves as a potential entry point for the development of novel Fe analogues of known complexes while exercising fine-tuned steric and electronic control over the Fe–macrocyclic core.

2. Experimental

The CTMC macrocycle was synthesized as described in the literature (Kolinski & Korybut-Daszkiewicz, 1975; Mash *et al.*, 2019; Tahirov *et al.*, 1995*a*). Consistent with previous structure determinations of the free ligand (Tahirov *et al.*, 1995*a*), we found evidence for the presence of at least two stereoisomers of CTMC (**A** is 5*SR*,7*RS*,12*SR*,14*RS* and **B** is 5*SR*,7*RS*,12*SR*,14*RS*), confirmed by the structures determined for the resulting Fe^{III} complexes reported herein. Two batches of CTMC were used to generate the *trans* and *cis* iron CTMC chloride species, with **A** being dominant in batch one (m.p. 178–181 °C) and **B** dominant in batch two (m.p. 70–135 °C). Altering the experimental method did not seem to allow for control over the presence of either stereoisomer of CTMC, and attempts to separate **A** and **B** were unfruitful. This lack of selectivity is consistent with the reported cocrystallization of **A** and **B** from the same synthesis (Tahirov *et al.*, 1995*a*). All commercially available materials were used as received. The IR spectra (ATR) of **1a**, **1b**, and **2** as powders were collected on a JASCO FT–IR 6300 instrument equipped with a diamond crystal. Magnetic measurements were conducted using a Johnson Matthey Magnetic Susceptibility Balance. Electronspray ionization mass spectrometry experiments were performed with an Advion Mass Spectrometer.

2.1. Synthesis and crystallization

2.1.1. Synthesis of *trans*-[Fe(CTMC)Cl_2][$FeCl_4$]/Cl (1a/1b). CTMC (0.449 g, 1.75 mmol, batch one) was dissolved in a 2:1 (*v*/*v*) dimethylformamide–triethyl orthoformate mixture

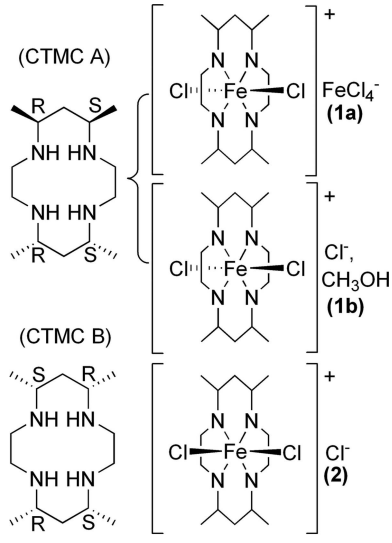

Figure 1
Stereoisomers of CTMC (left) and the resulting iron coordination complexes (right) discussed herein.

Table 1
Experimental details.

For all structures: $Z = 4$. Experiments were carried out at 150 K using a Bruker AXS D8 Quest diffractometer with a PhotonII charge-integrating pixel array detector (CPAD). Absorption was corrected for by multi-scan methods (*SADABS*; Krause *et al.*, 2015).

	1a	**1b**	**2**
Crystal data			
Chemical formula	$[Fe(C_{14}H_{32}N_4)Cl_2][FeCl_4]$	$[Fe(C_{14}H_{32}N_4)Cl_2]Cl{\cdot}CH_4O$	$[Fe(C_{14}H_{32}N_4)Cl_2]Cl$
M_r	580.83	450.68	418.63
Crystal system, space group	Monoclinic, $C2/c$	Monoclinic, $P2_1/c$	Orthorhombic, $Pbcn$
a, b, c (Å)	20.3512 (13), 6.4815 (4), 18.049 (1)	8.1632 (4), 20.8470 (12), 12.1387 (7)	9.2912 (12), 11.9579 (19), 17.267 (3)
α, β, γ (°)	90, 100.452 (3), 90	90, 95.024 (2), 90	90, 90, 90
V (Å^3)	2341.3 (2)	2057.8 (2)	1918.4 (5)
Radiation type	Mo $K\alpha$	Mo $K\alpha$	Cu $K\alpha$
μ (mm^{-1})	1.93	1.13	10.15
Crystal size (mm)	0.20 × 0.20 × 0.20	0.34 × 0.10 × 0.09	0.12 × 0.08 × 0.05
Data collection			
T_{min}, T_{max}	0.656, 0.747	0.679, 0.747	0.526, 0.754
No. of measured, independent and observed [$I > 2\sigma(I)$] reflections	71685, 4483, 3561	125711, 7859, 6505	14150, 2055, 1324
R_{int}	0.074	0.049	0.082
$(\sin \theta/\lambda)_{max}$ (Å^{-1})	0.771	0.770	0.638
Refinement			
$R[F^2 > 2\sigma(F^2)]$, $wR(F^2)$, S	0.027, 0.067, 1.02	0.024, 0.061, 1.04	0.066, 0.196, 1.08
No. of reflections	4483	7859	2055
No. of parameters	148	235	196
No. of restraints	15	0	273
H-atom treatment	H atoms treated by a mixture of independent and constrained refinement	H atoms treated by a mixture of independent and constrained refinement	H-atom parameters constrained
$\Delta\rho_{max}$, $\Delta\rho_{min}$ (e Å^{-3})	0.43, −0.48	0.70, −0.58	0.58, −0.95

Computer programs: *APEX3* (Bruker, 2019), *SAINT* (Bruker, 2019), *SHELXT2014* (Sheldrick, 2015*a*), *SHELXT* (Sheldrick, 2015*a*), *SHELXL2018* (Sheldrick, 2015*b*), *SHELXLE* (Hübschle *et al.*, 2011), *Mercury* (Macrae *et al.*, 2020), and *publCIF* (Westrip, 2010).

(30 ml) prior to purging with nitrogen. The mixture was stirred and heated while $FeCl_2{\cdot}4H_2O$ (0.697 g, 3.50 mmol) was dissolved in a 4:3 (*v*/*v*) dimethylformamide–triethyl orthoformate mixture (35 ml), previously purged with nitrogen, and was also left to stir and heat. The CTMC solution was transferred to the iron-containing flask *via* a cannula and the reaction was left to stir at 50 °C for 1 h. The reaction mixture was then exposed to oxygen and about 2 ml of concentrated hydrochloric acid were added dropwise to the flask while bubbling through oxygen. An additional 3 ml of concentrated hydrochloric acid were subsequently added, along with excess diethyl ether. A yield of 0.333 g of green powder was recovered *via* filtration and crystals of **1a** (space group $C2/c$; orange blocks) and **1b** ($P2_1/c$; yellow needles) were grown *via* slow diffusion of diethyl ether into a concentrated methanol solution of the product. ESI–MS: $[M]^+$, 381.9 ($^{35}Cl_2$), 384.0 (^{35}Cl, ^{37}Cl). IR (cm^{-1}): N—H 3174 (*m*), 3116 (*m*). μ_{eff} = 4.6 μ_B for the mixture of **1a/1b**, assuming a molecular weight of 418.63 g for $[Fe(CTMC)Cl_2]Cl$.

2.1.2. Synthesis of *cis*-$[Fe(CTMC)_2]Cl$ (2). CTMC (0.199 g, 0.775 mmol, batch two) was dissolved in a 3:1 (*v*/*v*) dimethylformamide–triethyl orthoformate solution (16 ml) and then purged with nitrogen. In a second flask, $FeCl_2{\cdot}4H_2O$ (0.311 g, 1.57 mmol) was dissolved in about 17 ml of a 2:1 (*v*/*v*) dimethylformamide–triethyl orthoformate solution and the resulting solution was purged with nitrogen. Both solutions were warmed and the CTMC solution was transferred *via* cannula to the iron material flask and the reaction mixture was left to stir under nitrogen at 55 °C for 45 min. Oxygen was then bubbled through the solution while 1 ml of concentrated hydrochloric acid was added. The slurry which formed was left to stir at room temperature for 2 h and 0.126 g of orange powder was obtained after filtration and washing with diethyl ether (30.1% yield). Compound **2** crystallized in the space group $Pbcn$ from the slow diffusion of acetone into an aqueous solution of the product. ESI–MS: $[M]^+$, 382.0 ($^{35}Cl_2$), 384.0 (^{35}Cl,^{37}Cl). IR (cm^{-1}): N—H 3073 (*m*), 3125 (*sh*). μ_{eff} = 5.6 μ_B.

2.2. Refinement

Crystal data, data collection and structure refinement details are summarized in Table 1. H atoms were placed in calculated positions, riding on the parent atom, except for the amine H atoms of **1a** (H1 and H2) and **1b** (H1–H4), which were refined. Methyl and hydroxy (methanol) groups were permitted to rotate. U_{iso}(H) values were set to a multiple of U_{eq}(C,N,O), with 1.5 for CH_3 and OH, and 1.2 for CH, CH_2, and NH units, respectively. The Fe atom of the $FeCl_4^-$ counter-anion in **1a** was modeled with very minor disorder over two positions (both located on twofold rotation axes) with close to identical but slightly shifted positions for the Cl atoms. The anisotropic displacement parameters (ADPs) of the Fe atoms (related by a half unit-cell shift with identical orientations) were constrained to be identical. U^{ij} components

Table 2
Selected geometric parameters (Å, °) for **1a**, **1b**, and **2**.

Bond lengths	1a	1b	2	Bond angles	1a	1b	2
Fe1—Cl1	2.2710 (3)	2.3084 (3)	2.3018 (15)	N1—Fe1—N2	85.21 (4)	85.23 (3)	86.85 (15)
Fe1—Cl2	–	2.3047 (3)	–	N1—Fe1—N2^{i,ii}	94.79 (4)	–	80.87 (16)
Fe1—N1	2.0276 (11)	2.0826 (9)	2.213 (4)	N1—Fe1—N4	–	94.13 (3)	–
Fe1—N2	2.0203 (11)	2.0787 (9)	2.154 (4)	N2—Fe1—N3	–	94.69 (3)	–
Fe1—N3	–	2.0654 (8)	–	N3—Fe1—N4	–	85.96 (3)	–
Fe1—N4	–	2.0761 (8)	–	Cl1—Fe1—Cl1^{i,ii†}	180.0	179.012 (11)	91.97 (8)

Symmetry code for **2**: (i) $-x, y, -z+\frac{1}{2}$; for **1a**: (ii) $-x+\frac{1}{2}, -y+\frac{3}{2}, -z+1$. † Compound **1b**: Cl2—Fe1—Cl1.

of ADPs for the Cl atoms were pairwise restrained to be similar (using a SIMU restraint with both s.u. values set to 0.01 Å^2). The occupancy ratio refined to 0.9803 (7):0.0197 (7). The cationic moiety of **2** exhibits disorder about a *pseudo*-mirror plane through the metal center. Both disordered moieties have crystallographic twofold symmetry with half the cation within the asymmetric unit. Exempt from the disorder are the Fe atom and the noncoordinated chloride counter-anion (Cl2). The disordered moieties were restrained to have similar anisotropic displacement parameters and 1,2 and 1,3 bond distances and angles. The C1—N1 and C1*B*—N1*B* bond lengths required additional restraints. The occupancy ratio refined to 0.944 (3):0.056 (3). Notably, the minor disordered moiety maintains the hydrogen-bonding network evident between the major cationic moiety and the chloride counter-anion (*vide infra*), which may facilitate the presence of the minor moiety.

2.3. Computational details

The cationic portions of **1** and **2** were optimized from the crystallographic coordinates of **1a** and **2** (counter-anions were omitted) in the *GAUSSIAN16* suite (Frisch *et al.*, 2016) using density functional theory (DFT) under vacuum, with the B3LYP functional (Becke, 1993) and Def2-SVP basis set (Weigend & Ahlrichs, 2005). The experimental magnetic moment of **1a**/**1b** (*vide supra*) is ambiguous, particularly given the presence of $FeCl_4^-$; therefore, both high- and low-spin states were tested: the low-spin state was found to be lowest in energy for **1** and was thus used for all remaining calculations on structures with a planar macrocycle. It was only possible to optimize the high-spin state for **2** (consistent with the experimental magnetic moment); thus, this was the only spin state considered for structures with a folded macrocycle. *GaussView6* (Dennington *et al.*, 2016) was used to analyze the data and manipulate the structures to form intermediate stereoisomers, as discussed below (see Fig. 6 for relevant discussion).

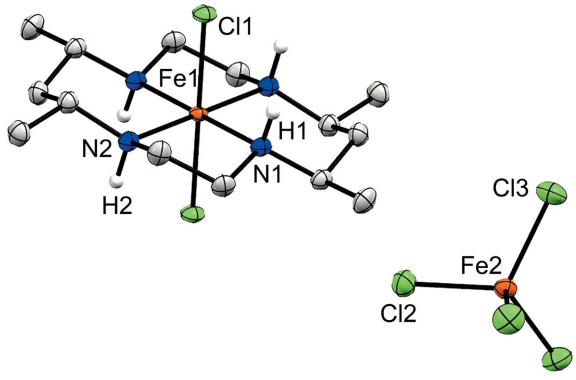

Figure 2
Displacement ellipsoid plot of **1a**. H atoms (except for those bound to N atoms) and the minor disordered $FeCl_4^-$ moiety have been omitted for clarity.

3. Results and discussion

Complex **1a** crystallized in the space group *C*2/*c* with the center of mass of the disordered $FeCl_4^-$ counter-anion lying on a twofold rotation axis, while the Fe atom of the macrocyclic moiety (Fe1) lies on an inversion center (Fig. 2). In contrast, no atoms lie on special positions in complex **1b**, which crystallized in the space group $P2_1/c$ (Fig. 3) with a methanol solvent molecule. Finally, complex **2** crystallized in the space group *Pbcn*, with both the chloride counter-anion and iron center lying on a twofold rotation axis (Fig. 4).

The Fe centers in all three complexes display a pseudo-octahedral geometry with four coordination sites occupied by the N atoms of the CTMC macrocycle and two by the chloride ligands. Additionally, regardless of *cis*- or *trans*-dichloro configuration, **1** and **2** both display similar Fe—Cl bond lengths ranging from 2.2710 (3) Å in **1a** to just greater than 2.30 Å in **1b** and **2** (see Table 2 for selected bond lengths and angles). As expected, each structure exhibits larger N—Fe—N bond angles between amines bridged by the $CH(Me)CH_2$-CH(Me) linkage and smaller angles between the CH_2CH_2 linkage of the macrocycle. Although the structural parameters

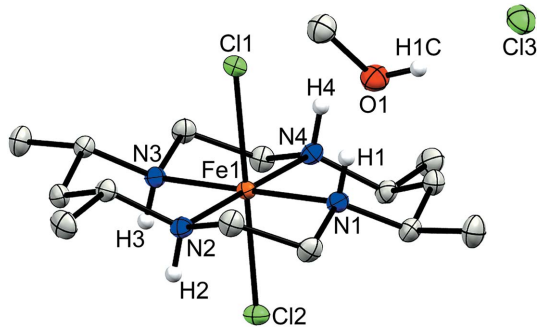

Figure 3
Displacement ellipsoid plot of **1b**. H atoms (except for those bound to N and methanolic O atoms) have been omitted for clarity.

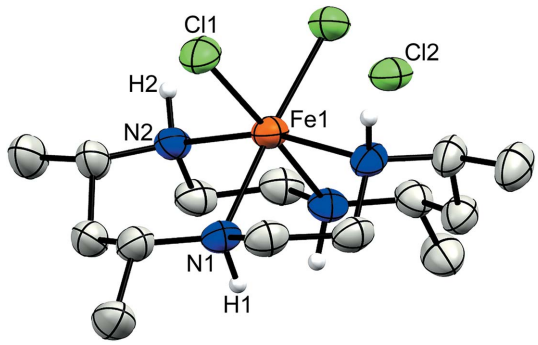

Figure 4
Displacement ellipsoid plot of **2**. H atoms (except for those bound to N atoms) and the minor disordered moiety have been omitted for clarity.

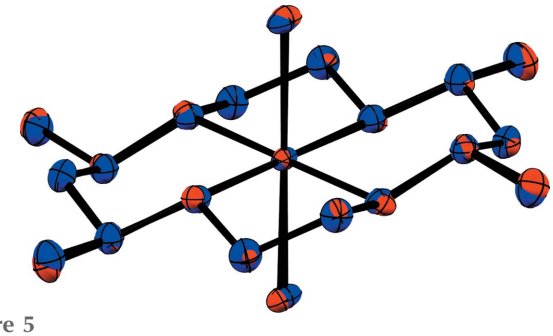

Figure 5
Least-squares overlay of **1a** (blue) and **1b** (red).

of the cation in **1b** are very similar to those of **1a**, the Fe—N and Fe—Cl bond lengths are slightly elongated in the former, which may be due to the differences in packing (*vide infra*). The least-squares overlay of **1a** and **1b** (Fig. 5) illustrates the general similarity of the cationic moieties. Both **1b** and **2** possess a noncoordinated chloride counter-ion, while **1a** contains a tetrachloridoferrate ion. As noted in the *Experimental* (Section 2), **2** was crystallized with the cationic portion disordered over two positions *via* a *pseudo*-mirror plane. As the second moiety accounts for only 5.6 (3)% of the occupancy and its bond lengths and angles were restrained to match that of the major moiety, it is not considered in the general bond length and angle comparisons.

The CTMC macrocycle appears as stereoisomers **A** and **B** (Fig. 1), as noted above. It is clear from the structures of **1a**, **1b**, and **2** that **A** tends to yield an iron complex in the *trans* configuration (**1a**/**1b**), while **B** tends to yield a complex in the *cis* configuration (**2**). To the best of our knowledge, the structure of **2** is the only example of a CTMC complex of **B**, and the only structure of a complex with a folded CTMC macrocycle. As seen in Table 2, the Fe—N bond lengths are consistently longer for **2** [2.154 (4)–2.213 (4) Å] compared to **1a** [2.0203 (11)–2.0276 (11) Å] and **1b** [2.0654 (8)–2.0826 (9) Å]. The N—Fe—N bond angles in **2** also deviate further from the ideal octahedral geometry of 90° than the same bond angles in **1a** and **1b**. Overall, the data suggest that the folded macrocycle conformation in **2** results in some strain compared to the planar coordination seen in **1a**/**1b**, favoring weaker Fe—N bonds.

To rationalize the preferences of a given stereoisomer for planar or folded coordination about the metal center, a series of DFT calculations were completed with **1a** as a low-spin complex and **2** as a high-spin complex in the gas phase. These calculations were completed by rotating one and then two methyl groups on the CTMC macrocycle, effectively reversing the *R* or *S* designation of the methyl groups, until the macrocycle was converted into the other observed stereoisomer (*i.e.* **A** into **B** and *vice versa*).

The DFT calculations indicate that the energy of the *cis* and *trans* configurations are indeed related to the stereoisomer of the macrocycle. A *trans* complex with **B** [Fig. 6(*c*)] is calculated to have an energy nearly 0.36 eV greater than that of a *trans* complex with **A** [*i.e.* **1a**/**1b**; Fig. 6(*a*)]. Forcing **A** to assume a folded conformation about the metal center [Fig. 6(*f*)] results in a calculated energy nearly 0.34 eV higher than that of the folded coordination of stereoisomer **B**. The energies of all *trans*-dichloro structures [Figs. 6(*a*)–(*c*)] are calculated to be lower than those of all *cis*-dichloro structures [Figs. 6(*d*)–(*f*)]. However, this is likely an artifact due to the different spin states (see *Experimental*, Section 2) assigned for the *trans* (*a*–*c*, $S = 1/2$) and *cis* (*d*–*f*, $S = 5/2$) geometries. Moreover, these gas-phase calculations neglect the counter-anions, with which the cations interact substantially in the solid state (*vide infra*). Nevertheless, the stepwise trends within each geometric series (*a*–*c* and *d*–*f*) clearly illustrate the dependence of the energy of the planar and folded coordination modes on the stereoisomer of CTMC. Consistent with **1a**/**1b**, **A** clearly prefers a planar coordination geometry. In contrast, a folded macrocycle is most easily obtained with **B**, consistent with the structure of **2**. These energetic preferences are most reasonably attributed to the effect of the methyl substituents, which lean towards the arrangement of minimal steric interactions. This is consistent with reports on metal complexes of HMC, for which a strong preference of the stereoisomers to form *cis* or *trans* metal

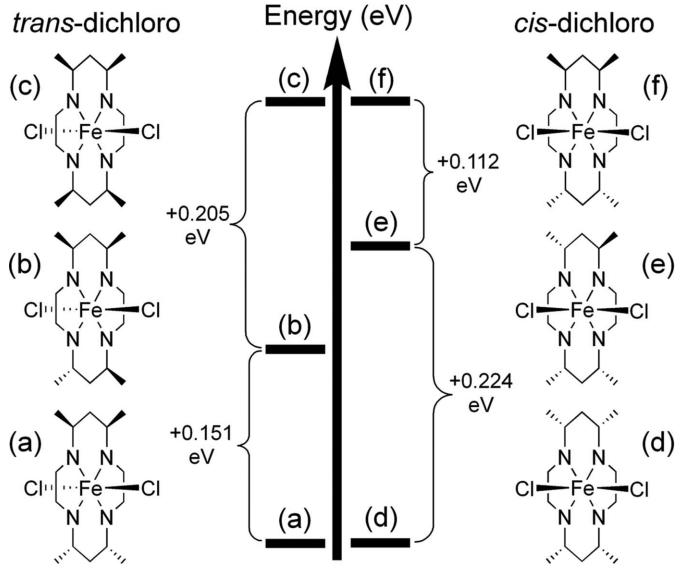

Figure 6
DFT-derived energetic orderings for complexes of various isomers of CTMC in planar (left) or folded (right) conformations.

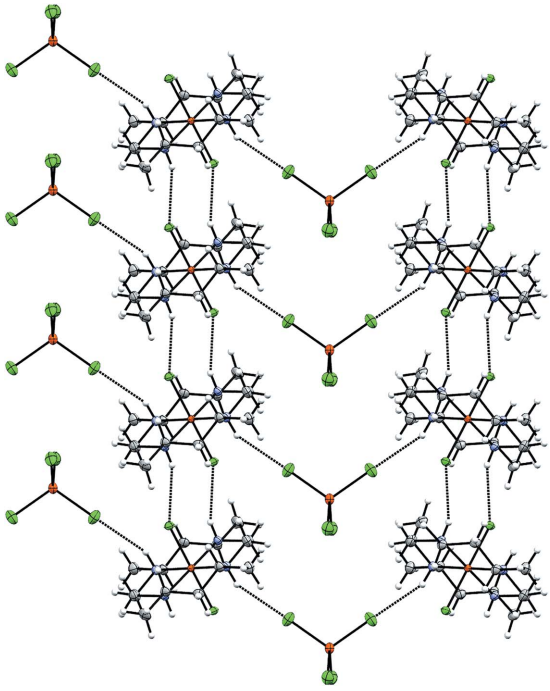

Figure 7
Illustration of the hydrogen-bonding interactions in **1a**.

complexes is well established (Clendening *et al.*, 2019; House *et al.*, 1983; Tyler *et al.*, 2016).

The previously reported data for *cis*/*trans*-[Fe^{III}(cyclam)-Cl_2]$^+$ and *cis*/*trans*-[Fe^{III}(HMC)Cl_2]$^+$ are useful for the discussion pertaining to planar *versus* folded macrocycles (Clendening *et al.*, 2019; Guilard *et al.*, 1997). As with iron–CTMC, the Fe—Cl bond lengths of these Fe^{III} complexes remain similar to one another regardless of a *cis* or *trans* nature. These complexes display Fe—Cl bond lengths ranging from 2.27 to 2.32 Å, with no significant dependence on the coordination geometry of the macrocycle. In contrast, the Fe—N bond lengths for all of the complexes confirm the trends observed for **1a**/**1b** *versus* **2**. Similar to the difference (0.16 Å) between **1a** and **2**, the averaged Fe—N bond lengths of *cis*-[Fe^{III}(cyclam)Cl_2]$^+$ and *cis*-[Fe^{III}(HMC)Cl_2]$^+$ are roughly 0.16 and 0.17 Å longer than those of *trans*-[Fe^{III}(cyclam)Cl_2]$^+$ and *trans*-[Fe^{III}(HMC)Cl_2]$^+$, respectively. The N—Fe—N angles of **1a**, *trans*-[Fe^{III}(cyclam)Cl_2]$^+$, and *trans*-[Fe^{III}(HMC)-Cl_2]$^+$ round to 85° between the CH_2CH_2 linkage and 95° between the $CR_2CH_2CR_2$ linkage. The N—Fe—N bond angles for the complexes with folded macrocycles vary from 79.56 (8) to 81.55 (5)° between the CH_2CH_2 linkage and from 83.15 (5) to 86.85 (15)° between the $CR_2CH_2CR_2$ linkage. In short, each *cis* complex exhibits longer Fe—N bond lengths and N—Fe—N bond angles which deviate further from an ideal octahedral coordination geometry than in the respective *trans* complexes.

It is further possible to compare the structural parameters as the number of methyl groups is systematically varied within either the *cis* or *trans* series. The averaged Fe—N bond lengths of *cis*-[Fe^{III}(HMC)Cl_2]Cl (*ca* 2.21 Å) appears longer than those of **2** and *cis*-[Fe^{III}(cyclam)Cl_2]Cl (both *ca* 2.18 Å) (Clendening *et al.*, 2019; Guilard *et al.*, 1997), which is likely due to the steric bulk of the two methyl groups at the same position of the macrocycle (*e.g.* 5,5 and 12,12), which forces at least one methyl group to be axially oriented. For the *trans* structures, a continuous increase in the averaged Fe—N bond lengths may be observed from *trans*-[Fe^{III}(cyclam)Cl_2]$FeCl_4$ (2.006 Å) to **1a** (2.024 Å) to *trans*-[Fe^{III}(HMC)Cl_2]$FeCl_4$ (2.054 Å) (Clendening *et al.*, 2019; Guilard *et al.*, 1997). Although methyl groups are electron rich and would thus be expected to slightly increase the donor strength of the macrocycle towards the electron-poor Fe^{III} center, it appears that steric effects dominate, resulting in a progressively weaker Fe—N bond with increasing number of macrocylic substituents.

The packing in **1a** is strikingly similar to *trans*-[Fe^{III}-(HMC)Cl_2]$FeCl_4$ (Clendening *et al.*, 2019) and *trans*-[Fe^{III}-(cyclam)Cl_2]$FeCl_4$ (Guilard *et al.*, 1997), despite the differences in space group ($C2/c$, $P2_1/c$, and $P2_1/n$, respectively). The cationic units in all cases pack in a series of columns (see Fig. 7), each linked to the preceding and following unit by two hydrogen bonds between the amine groups and the chloride ligands (N1 and Cl1 in the case of **1a**). The remaining unique

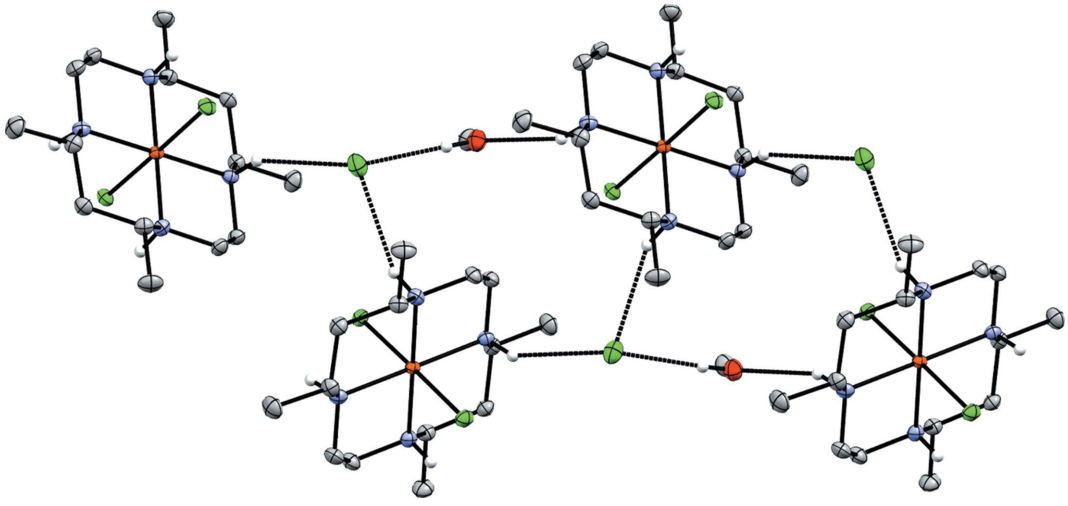

Figure 8
Illustration of the hydrogen-bonding interactions in **1b**.

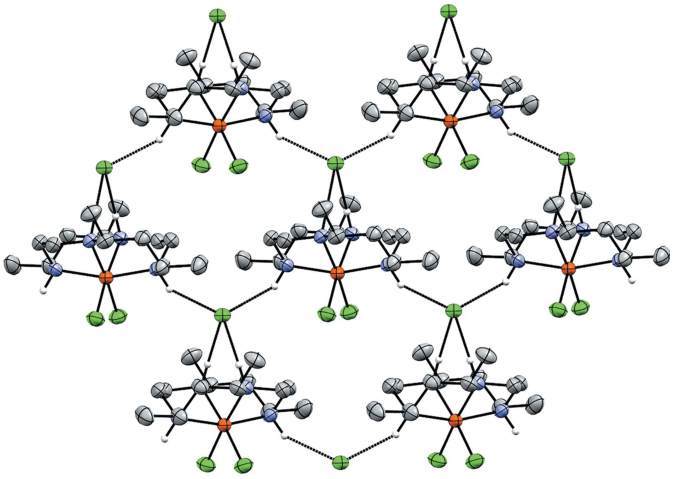

Figure 9
Illustration of the hydrogen-bonding interactions in **2**.

amine position(s) (N2 in **1a**) instead participates in hydrogen-bonding interactions with the $FeCl_4^-$ units (*via* Cl3 in **1a**), which are also arranged in columns. This similarity suggests that the common tetrachloridoferrate counter-anion may be favored due to this ability to participate in extensive hydrogen-bonding networks with the ferric chloride complexes bearing planar macrocycles. The minor disordered counter-anion of **1a** has the same hydrogen-bonding interactions as its major counterpart.

Lacking the $FeCl_4^-$ counter-anion, complex **1b** ($P2_1/c$) packs differently, forming infinite chains parallel to [001] connected *via* hydrogen bonds with one cation, one chloride counter-anion, and one methanol solvent molecule as the repeat unit that are related to each other *via* one of the glide plane(s) (see Fig. 8). In between the glide planes and between neighboring chains, the molecules are instead related by inversion. Interestingly, and in sharp contrast to the case of **1a** and its structural relatives, there are in **1b** no direct hydrogen bonds between the cationic moieties (N1 is instead hydrogen bonded to the methanol solvent molecule and N3 and N4 to the chloride counter-anion), and both of the chloride ligands and one of the amine positions (N2) in **1b** do not participate in hydrogen bonding at all.

This illustrates the difficulty of a single chloride counter-anion to effectively facilitate the hydrogen bonding within the *trans* orientation of these complexes, apparently necessitating the solvent inclusion and further supporting the conjecture that the inclusion of $FeCl_4^-$ in the crystal structures is favored by its ability to facilitate ordered packing in the resulting solid. The packing differences may also hint at a supramolecular origin for the elongated Fe—Cl and Fe—N bond lengths of the cationic moieties of **1b** *versus* **1a**, as the latter engages in more extensive hydrogen bonding (six hydrogen bonds per $\mathbf{1a}^+$ and three per $\mathbf{1b}^+$) which includes the chloride ligands, in contrast to **1b**.

The similarity of the hydrogen-bonding network among structural analogues extends to the cases of **2** (*Pbcn*), *cis*-[Fe^{III}(HMC)Cl_2]Cl (*Fdd*2), and *cis*-[Fe^{III}(cyclam)Cl_2]Cl ($P2_1/c$) (Clendening *et al.*, 2019; Guilard *et al.*, 1997). As with **1b**, neither of the chloride ligands participates in hydrogen bonding, nor do any of the cationic moieties hydrogen bond with each other. However, in all three of these structures with a folded macrocycle, a close network of hydrogen bonding is facilitated by the chloride counter-anion, which simultaneously participates in four such interactions with three separate cationic moieties (Fig. 9). Two hydrogen bonds occur with the amines of a single moiety which face into the cavity of the folded macrocycle (N1 and its symmetry equivalent in **2**). The remaining hydrogen bonds are formed from interactions with an outward-facing amine group of two separate moieties. Thus, in the case of the folded macrocycles, the large $FeCl_4^-$ anion is no longer necessary in order to stabilize an extended network of hydrogen bonds. Interestingly, the minor disordered moiety of **2** maintains these strong hydrogen-bonding networks, which perhaps facilitates the disorder about the *pseudo*-mirror plane in **2** (see Fig. 10).

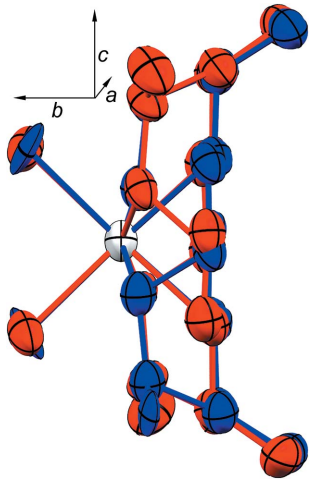

Figure 10
View of the major (red) and minor (blue) disordered moieties of **2** along the *a* axis, with the *b* axis oriented horizontally and the *c* axis vertically.

4. Conclusion

This article describes the structural properties of new ferric dichloride complexes of CTMC stereoisomers **A** (**1a**/**1b** – planar macrocycle) and **B** (**2** – folded macrocycle). DFT calculations are used to support the apparent preferences of **A** and **B** to form planar or folded coordination complexes, respectively. Moreover, comparison to related structures based on cyclam and HMC illustrate a strong dependence of the intermolecular hydrogen-bonding interactions on the macrocyclic coordination geometry [*i.e.* planar (*trans*-dichloro) or folded (*cis*-dichloro)]. Given the known reactivity dependence of a complex on its overall geometry, complexes **1a**, **1b**, and **2** demonstrate how control can be exercised over the geometric coordination isomer by the stereochemistry of as few as four methyl groups on the periphery of the macrocycle. This contrasts with the ability of cyclam (no methyl groups) to assume either folded or planar conformations (Guilard *et al.*, 1997), and compliments the rigid structural preferences ascribed to the stereoisomers of HMC, which

bears six methyl groups (Clendening *et al.*, 2019; House *et al.*, 1983; Tyler *et al.*, 2016). Work is underway to investigate derivatives of Fe(CTMC) with the goal of studying the charge-transfer excited states of such complexes.

Acknowledgements

This work is based on research supported by the US National Science Foundation. The grant holders acknowledge that opinions, findings, and conclusions or recommendations expressed in any publication generated by NSF-supported research are those of the authors and that the NSF accepts no liability whatsoever in this regard. SSD thanks Purdue University for a Summer Research Fellowship. Mr Randy Akrofi collected the diffraction data set for **1b**.

Funding information

Funding for this research was provided by: National Science Foundation (grant No. CHE 2102049 to TR for research; grant No. CHE 1625543 to TR and MZ for X-ray diffractometers).

References

Becke, A. D. (1993). *J. Chem. Phys.* **98**, 5648–5652.

Bruker (2019). *APEX3* and *SAINT*. Bruker AXS Inc., Madison, Wisconsin, USA.

Cao, Z., Forrest, W. P., Gao, Y., Fanwick, P. E. & Ren, T. (2012). *Organometallics*, **31**, 6199–6206.

Clendening, R. A. & Ren, T. (2022). *Eur. J. Inorg. Chem.* **2022**, e202101021.

Clendening, R. A., Zeller, M. & Ren, T. (2019). *Acta Cryst.* C**75**, 1509–1516.

Clendening, R. A., Zeller, M. & Ren, T. (2022). *Inorg. Chem.* **61**, 13442–13452.

Constable, E. C. (1999). In *Coordination Chemistry of Macrocyclic Compounds*. Oxford University Press.

Dennington, R., Keith, T. A. & Millam, J. M. (2016). *GaussView*. Version 6. Semichem Inc., Shawnee Mission, KS, USA.

Frisch, M. J., *et al.* (2016). *GAUSSIAN16*. Revision A.03. Gaussian Inc., Wallingford, CT, USA. https://gaussian.com/.

Guilard, R., Siri, O., Tabard, A., Broeker, G., Richard, P., Nurco, D. J. & Smith, K. M. (1997). *J. Chem. Soc. Dalton Trans.* pp. 3459–3463.

House, D. A., Hay, R. W. & Akbar Ali, M. (1983). *Inorg. Chim. Acta*, **72**, 239–245.

Hübschle, C. B., Sheldrick, G. M. & Dittrich, B. (2011). *J. Appl. Cryst.* **44**, 1281–1284.

Kolinski, R. A. & Korybut-Daszkiewicz, B. (1975). *Inorg. Chim. Acta*, **14**, 237–245.

Kottrup, K. G. & Hetterscheid, D. G. H. (2016). *Chem. Commun.* **52**, 2643–2646.

Krause, L., Herbst-Irmer, R., Sheldrick, G. M. & Stalke, D. (2015). *J. Appl. Cryst.* **48**, 3–10.

Macrae, C. F., Sovago, I., Cottrell, S. J., Galek, P. T. A., McCabe, P., Pidcock, E., Platings, M., Shields, G. P., Stevens, J. S., Towler, M. & Wood, P. A. (2020). *J. Appl. Cryst.* **53**, 226–235.

Mash, B. L., Raghavan, A. & Ren, T. (2019). *Eur. J. Inorg. Chem.* **2019**, 2065–2070.

Meyer, K., Bill, E., Mienert, B., Weyhermüller, T. & Wieghardt, K. (1999). *J. Am. Chem. Soc.* **121**, 4859–4876.

Prakash, J., Rohde, G. T., Meier, K. K., Münck, E. & Que, L. J. (2015). *Inorg. Chem.* **54**, 11055–11057.

Rohde, J.-U., In, J.-H., Lim, M. H., Brennessel, W. W., Bukowski, M. R., Stubna, A., Münck, E., Nam, W. & Que, L. J. (2003). *Science*, **299**, 1037–1039.

Sheldrick, G. M. (2015*a*). *Acta Cryst.* A**71**, 3–8.

Sheldrick, G. M. (2015*b*). *Acta Cryst.* C**71**, 3–8.

Straub, S. & Vöhringer, P. (2021). *Angew. Chem. Int. Ed.* **60**, 2519–2525.

Tahirov, T. H., Lu, T.-H., Liu, G.-S., Chi, T.-Y. & Chung, C.-S. (1995*a*). *Acta Cryst.* C**51**, 1146–1148.

Tahirov, T. H., Lu, T.-H., Liu, G.-S., Chi, T.-Y. & Chung, C.-S. (1995*b*). *Acta Cryst.* C**51**, 2018–2020.

Tyler, S. F., Judkins, E. C., Song, Y., Cao, F., McMillin, D. R., Fanwick, P. E. & Ren, T. (2016). *Inorg. Chem.* **55**, 8736–8743.

Wang, J.-W., Liu, W.-J., Zhong, D.-C. & Lu, T.-B. (2019). *Coord. Chem. Rev.* **378**, 237–261.

Weigend, F. & Ahlrichs, R. (2005). *Phys. Chem. Chem. Phys.* **7**, 3297–3305.

Westrip, S. P. (2010). *J. Appl. Cryst.* **43**, 920–925.

supporting information

Acta Cryst. (2022). C**78**, 507-514 [https://doi.org/10.1107/S205322962200849X]

Geometric isomers of dichloridoiron(III) complexes of CTMC (5,7,12,14-tetramethyl-1,4,8,11-tetraazacyclotetradecane)

Stephanie S. DeLancey, Reese A. Clendening, Matthias Zeller and Tong Ren

Computing details

For all structures, data collection: *APEX3* (Bruker, 2019); cell refinement: *SAINT* (Bruker, 2019); data reduction: *SAINT* (Bruker, 2019). Program(s) used to solve structure: SHELXT2014 (Sheldrick, 2015a) for (1a), (1b); SHELXT (Sheldrick, 2015a) for (2). For all structures, program(s) used to refine structure: *SHELXL2018* (Sheldrick, 2015b) and SHELXLE (Hübschle *et al.*, 2011); molecular graphics: *Mercury* (Macrae *et al.*, 2020); software used to prepare material for publication: *publCIF* (Westrip, 2010).

trans-Dichlorido[(5*SR*,7*RS*,12*RS*,14*SR*)-4,7,12,14-tetramethyl-1,4,8,11-tetraazacyclotetradecane]iron(III) tetrachloridoferrate (1a)

Crystal data

$[Fe(C_{14}H_{32}N_4)Cl_2][FeCl_4]$
M_r = 580.83
Monoclinic, $C2/c$
a = 20.3512 (13) Å
b = 6.4815 (4) Å
c = 18.049 (1) Å
β = 100.452 (3)°
V = 2341.3 (2) Å^3
Z = 4
$F(000)$ = 1192
D_x = 1.648 Mg m^{-3}
Mo $K\alpha$ radiation, λ = 0.71073 Å
Cell parameters from 9346 reflections
θ = 3.3–33.1°
μ = 1.93 mm^{-1}
T = 150 K
Block, orange
0.20 × 0.20 × 0.20 mm

Data collection

Bruker AXS D8 Quest diffractometer with PhotonII charge-integrating pixel array detector (CPAD)
Radiation source: fine focus sealed tube X-ray source
Triumph curved graphite crystal monochromator
Detector resolution: 7.4074 pixels mm^{-1}
ω and phi scans
Absorption correction: multi-scan (SADABS; Krause *et al.*, 2015)
T_{min} = 0.656, T_{max} = 0.747
71685 measured reflections
4483 independent reflections
3561 reflections with $I > 2\sigma(I)$
R_{int} = 0.074
θ_{max} = 33.2°, θ_{min} = 3.3°
$h = -31 \rightarrow 31$
$k = -9 \rightarrow 9$
$l = -27 \rightarrow 27$

Refinement

Refinement on F^2
Least-squares matrix: full
$R[F^2 > 2\sigma(F^2)]$ = 0.027
$wR(F^2)$ = 0.067
S = 1.02
4483 reflections
148 parameters
15 restraints

Hydrogen site location: mixed
H atoms treated by a mixture of independent and constrained refinement

$w = 1/[\sigma^2(F_o^2) + (0.0297P)^2 + 1.680P]$ where $P = (F_o^2 + 2F_c^2)/3$
$(\Delta/\sigma)_{max} = 0.001$
$\Delta\rho_{max} = 0.43$ e Å^{-3}
$\Delta\rho_{min} = -0.48$ e Å^{-3}

Special details

Geometry. All esds (except the esd in the dihedral angle between two l.s. planes) are estimated using the full covariance matrix. The cell esds are taken into account individually in the estimation of esds in distances, angles and torsion angles; correlations between esds in cell parameters are only used when they are defined by crystal symmetry. An approximate (isotropic) treatment of cell esds is used for estimating esds involving l.s. planes.

Refinement. The iron atom of the FeCl4 counteranion was modelled as having very minor disorder over two positions (both located on two-fold rotation axes) with close to identical but slightly shifted positions for the chlorine atoms. The ADPs of the Fe atoms (related by a half unit cell shift with identical orientations) were constrained to be identical. Uij components of ADPs for the chlorine atoms were pairwise restrained to be similar (using a SIMU restraint with both esds set to 0.01 Angstrom squared). The occupancy ratio refined to 0.9803 (7) to 0.0197 (7).

Fractional atomic coordinates and isotropic or equivalent isotropic displacement parameters (Å²)

	x	*y*	*z*	U_{iso}*/U_{eq}	Occ. (<1)
Fe2	0.500000	0.78720 (5)	0.250000	0.02099 (7)	0.9803 (7)
Cl2	0.43633 (2)	0.98293 (8)	0.30654 (3)	0.03295 (10)	0.9803 (7)
Cl3	0.56398 (3)	0.59283 (8)	0.33308 (3)	0.03643 (12)	0.9803 (7)
Fe2B	0.500000	0.295 (2)	0.250000	0.02099 (7)	0.0197 (7)
Cl2B	0.4455 (13)	0.065 (4)	0.3013 (16)	0.044 (5)	0.0197 (7)
Cl3B	0.5568 (16)	0.519 (4)	0.3227 (15)	0.036 (4)	0.0197 (7)
Fe1	0.250000	0.750000	0.500000	0.01337 (6)	
Cl1	0.24845 (2)	0.46489 (5)	0.57279 (2)	0.01997 (7)	
N1	0.24598 (6)	0.93617 (17)	0.58935 (6)	0.0171 (2)	
H1	0.2410 (8)	1.058 (3)	0.5698 (9)	0.021*	
N2	0.35008 (6)	0.76192 (17)	0.53443 (6)	0.0181 (2)	
H2	0.3592 (8)	0.642 (3)	0.5615 (10)	0.022*	
C1	0.31267 (7)	0.9338 (2)	0.63842 (7)	0.0220 (3)	
H1A	0.317297	0.809713	0.670954	0.026*	
H1B	0.318213	1.057391	0.671182	0.026*	
C2	0.36500 (7)	0.9320 (2)	0.58942 (8)	0.0233 (3)	
H2A	0.364878	1.065345	0.562640	0.028*	
H2B	0.409764	0.911880	0.620775	0.028*	
C3	0.39433 (7)	0.7600 (2)	0.47710 (8)	0.0210 (2)	
H3	0.386422	0.890263	0.447113	0.025*	
C5	0.37661 (7)	0.5783 (2)	0.42328 (8)	0.0224 (3)	
H5A	0.412631	0.562226	0.393511	0.027*	
H5B	0.375954	0.451418	0.453672	0.027*	
C6	0.31013 (7)	0.5939 (2)	0.36869 (7)	0.0196 (2)	
H6	0.306426	0.736177	0.346859	0.024*	
C4	0.46790 (7)	0.7525 (2)	0.51366 (9)	0.0259 (3)	
H4A	0.495428	0.748858	0.474401	0.039*	
H4B	0.476420	0.628507	0.545009	0.039*	
H4C	0.479181	0.875264	0.545082	0.039*	

C7	0.30763 (8)	0.4401 (2)	0.30396 (8)	0.0270 (3)
H7A	0.345957	0.462984	0.279012	0.041*
H7B	0.266122	0.459639	0.267536	0.041*
H7C	0.309221	0.299169	0.323860	0.041*

Atomic displacement parameters (Å²)

	U^{11}	U^{22}	U^{33}	U^{12}	U^{13}	U^{23}
Fe2	0.02090 (14)	0.02448 (15)	0.01653 (13)	0.000	0.00055 (10)	0.000
Cl2	0.0332 (2)	0.0394 (3)	0.02645 (18)	0.0078 (2)	0.00606 (16)	−0.00410 (19)
Cl3	0.0380 (3)	0.0370 (3)	0.0316 (2)	0.0082 (2)	−0.00105 (18)	0.0104 (2)
Fe2B	0.02090 (14)	0.02448 (15)	0.01653 (13)	0.000	0.00055 (10)	0.000
Cl2B	0.036 (8)	0.045 (9)	0.043 (8)	−0.011 (8)	−0.017 (7)	0.017 (8)
Cl3B	0.048 (8)	0.022 (8)	0.035 (8)	−0.013 (7)	−0.002 (7)	0.009 (7)
Fe1	0.01769 (12)	0.01052 (11)	0.01146 (10)	0.00053 (8)	0.00149 (8)	0.00009 (8)
Cl1	0.02917 (16)	0.01303 (13)	0.01735 (13)	0.00079 (11)	0.00326 (11)	0.00235 (10)
N1	0.0219 (5)	0.0147 (5)	0.0145 (4)	−0.0005 (4)	0.0027 (4)	−0.0011 (4)
N2	0.0198 (5)	0.0175 (5)	0.0168 (5)	−0.0004 (4)	0.0029 (4)	−0.0009 (4)
C1	0.0241 (6)	0.0252 (6)	0.0155 (5)	−0.0013 (5)	0.0004 (5)	−0.0045 (5)
C2	0.0222 (6)	0.0267 (7)	0.0200 (6)	−0.0033 (5)	0.0011 (5)	−0.0068 (5)
C3	0.0212 (6)	0.0219 (6)	0.0200 (6)	0.0005 (5)	0.0043 (5)	−0.0019 (5)
C5	0.0238 (6)	0.0219 (6)	0.0221 (6)	0.0032 (5)	0.0058 (5)	−0.0029 (5)
C6	0.0242 (6)	0.0185 (6)	0.0167 (5)	−0.0002 (5)	0.0054 (5)	−0.0018 (4)
C4	0.0202 (6)	0.0297 (7)	0.0277 (7)	−0.0008 (5)	0.0042 (5)	−0.0009 (6)
C7	0.0333 (8)	0.0279 (7)	0.0217 (6)	−0.0021 (6)	0.0101 (6)	−0.0074 (5)

Geometric parameters (Å, º)

Fe2—Cl2	2.1931 (5)	C1—C2	1.5028 (19)
Fe2—Cl2^{i}	2.1932 (5)	C1—H1A	0.9900
Fe2—Cl3^{i}	2.1960 (5)	C1—H1B	0.9900
Fe2—Cl3	2.1961 (5)	C2—H2A	0.9900
Fe2B—Cl3B^{i}	2.147 (16)	C2—H2B	0.9900
Fe2B—Cl3B	2.147 (16)	C3—C4	1.523 (2)
Fe2B—Cl2B^{i}	2.164 (16)	C3—C5	1.5275 (19)
Fe2B—Cl2B	2.164 (16)	C3—H3	1.0000
Fe1—N2^{ii}	2.0203 (11)	C5—C6	1.5257 (19)
Fe1—N2	2.0203 (11)	C5—H5A	0.9900
Fe1—N1	2.0276 (11)	C5—H5B	0.9900
Fe1—N1^{ii}	2.0276 (11)	C6—C7	1.5297 (18)
Fe1—Cl1^{ii}	2.2709 (3)	C6—H6	1.0000
Fe1—Cl1	2.2710 (3)	C4—H4A	0.9800
N1—C1	1.4802 (17)	C4—H4B	0.9800
N1—C6^{ii}	1.4933 (17)	C4—H4C	0.9800
N1—H1	0.862 (18)	C7—H7A	0.9800
N2—C2	1.4776 (17)	C7—H7B	0.9800
N2—C3	1.4900 (17)	C7—H7C	0.9800
N2—H2	0.917 (18)		

Cl2—Fe2—Cl2^{i}	109.32 (3)	N1—C1—H1B	110.0
Cl2—Fe2—Cl3^{i}	108.81 (2)	C2—C1—H1B	110.0
Cl2^{i}—Fe2—Cl3^{i}	109.96 (2)	H1A—C1—H1B	108.4
Cl2—Fe2—Cl3	109.96 (2)	N2—C2—C1	108.65 (11)
Cl2^{i}—Fe2—Cl3	108.81 (2)	N2—C2—H2A	110.0
Cl3^{i}—Fe2—Cl3	109.99 (3)	C1—C2—H2A	110.0
Cl3B^{i}—Fe2B—Cl3B	95.0 (17)	N2—C2—H2B	110.0
Cl3B^{i}—Fe2B—Cl2B	117.8 (12)	C1—C2—H2B	110.0
Cl3B—Fe2B—Cl2B	117.7 (11)	H2A—C2—H2B	108.3
Cl2B^{i}—Fe2B—Cl2B	93 (2)	N2—C3—C4	111.70 (11)
N2^{ii}—Fe1—N2	180.0	N2—C3—C5	110.20 (11)
N2^{ii}—Fe1—N1	94.79 (4)	C4—C3—C5	110.55 (11)
N2—Fe1—N1	85.21 (4)	N2—C3—H3	108.1
N2^{ii}—Fe1—N1^{ii}	85.21 (4)	C4—C3—H3	108.1
N2—Fe1—N1^{ii}	94.79 (4)	C5—C3—H3	108.1
N1—Fe1—N1^{ii}	180.0	C6—C5—C3	116.04 (11)
N2^{ii}—Fe1—Cl1^{ii}	88.41 (3)	C6—C5—H5A	108.3
N2—Fe1—Cl1^{ii}	91.59 (3)	C3—C5—H5A	108.3
N1—Fe1—Cl1^{ii}	89.01 (3)	C6—C5—H5B	108.3
N1^{ii}—Fe1—Cl1^{ii}	90.99 (3)	C3—C5—H5B	108.3
N2^{ii}—Fe1—Cl1	91.59 (3)	H5A—C5—H5B	107.4
N2—Fe1—Cl1	88.41 (3)	N1^{ii}—C6—C5	109.50 (10)
N1—Fe1—Cl1	90.99 (3)	N1^{ii}—C6—C7	112.31 (11)
N1^{ii}—Fe1—Cl1	89.01 (3)	C5—C6—C7	110.66 (11)
Cl1^{ii}—Fe1—Cl1	180.0	N1^{ii}—C6—H6	108.1
C1—N1—C6^{ii}	113.43 (10)	C5—C6—H6	108.1
C1—N1—Fe1	107.75 (8)	C7—C6—H6	108.1
C6^{ii}—N1—Fe1	118.07 (8)	C3—C4—H4A	109.5
C1—N1—H1	106.4 (11)	C3—C4—H4B	109.5
C6^{ii}—N1—H1	106.4 (11)	H4A—C4—H4B	109.5
Fe1—N1—H1	103.7 (11)	C3—C4—H4C	109.5
C2—N2—C3	113.35 (11)	H4A—C4—H4C	109.5
C2—N2—Fe1	107.94 (8)	H4B—C4—H4C	109.5
C3—N2—Fe1	119.26 (8)	C6—C7—H7A	109.5
C2—N2—H2	106.0 (11)	C6—C7—H7B	109.5
C3—N2—H2	105.9 (10)	H7A—C7—H7B	109.5
Fe1—N2—H2	103.1 (11)	C6—C7—H7C	109.5
N1—C1—C2	108.58 (11)	H7A—C7—H7C	109.5
N1—C1—H1A	110.0	H7B—C7—H7C	109.5
C2—C1—H1A	110.0		

C6^{ii}—N1—C1—C2	171.29 (11)	C2—N2—C3—C5	179.08 (11)
Fe1—N1—C1—C2	38.66 (13)	Fe1—N2—C3—C5	−52.15 (13)
C3—N2—C2—C1	173.45 (11)	N2—C3—C5—C6	70.58 (15)
Fe1—N2—C2—C1	39.08 (13)	C4—C3—C5—C6	−165.46 (12)
N1—C1—C2—N2	−52.20 (15)	C3—C5—C6—N1^{ii}	−72.54 (15)

C2—N2—C3—C4	55.78 (15)	C3—C5—C6—C7	163.13 (12)
Fe1—N2—C3—C4	−175.44 (9)		

Symmetry codes: (i) −*x*+1, *y*, −*z*+1/2; (ii) −*x*+1/2, −*y*+3/2, −*z*+1.

Hydrogen-bond geometry (Å, º)

D—H···*A*	*D*—H	H···*A*	*D*···*A*	*D*—H···*A*
N2—H2···Cl3^{a}iii	0.917 (18)	2.704 (18)	3.5421 (12)	152.5 (14)
N2—H2···Cl3^{B}b^{iii}	0.917 (18)	2.66 (3)	3.43 (3)	142.1 (14)
N1—H1···Cl1^{iv}	0.862 (18)	2.643 (18)	3.4411 (12)	154.5 (14)

Symmetry codes: (iii) −*x*+1, −*y*+1, −*z*+1; (iv) *x*, *y*+1, *z*.

trans-Dichlorido[(5*SR*,7*RS*,12*RS*,14*SR*)-4,7,12,14-tetramethyl-1,4,8,11-tetraazacyclotetradecane]iron(III) chloride methanol monosolvate (1b)

Crystal data

$[Fe(C_{14}H_{32}N_4)Cl_2]Cl\cdot CH_4O$
M_r = 450.68
Monoclinic, $P2_1/c$
a = 8.1632 (4) Å
b = 20.8470 (12) Å
c = 12.1387 (7) Å
β = 95.024 (2)°
V = 2057.8 (2) Å^3
Z = 4
$F(000)$ = 956
D_x = 1.455 Mg m^{-3}
Mo $K\alpha$ radiation, λ = 0.71073 Å
Cell parameters from 9046 reflections
θ = 2.6–33.1°
μ = 1.13 mm^{-1}
T = 150 K
Needle, yellow
0.34 × 0.10 × 0.09 mm

Data collection

Bruker AXS D8 Quest diffractometer with PhotonII charge-integrating pixel array detector (CPAD)
Radiation source: fine focus sealed tube X-ray source
Triumph curved graphite crystal monochromator
Detector resolution: 7.4074 pixels mm^{-1}
ω and phi scans
Absorption correction: multi-scan (SADABS; Krause *et al.*, 2015)
T_{min} = 0.679, T_{max} = 0.747
125711 measured reflections
7859 independent reflections
6505 reflections with $I > 2\sigma(I)$
R_{int} = 0.049
θ_{max} = 33.2°, θ_{min} = 2.7°
h = −12→12
k = −32→32
l = −18→18

Refinement

Refinement on F^2
Least-squares matrix: full
$R[F^2 > 2\sigma(F^2)]$ = 0.024
$wR(F^2)$ = 0.061
S = 1.04
7859 reflections
235 parameters
0 restraints
Primary atom site location: dual
Secondary atom site location: difference Fourier map
Hydrogen site location: mixed
H atoms treated by a mixture of independent and constrained refinement
$w = 1/[\sigma^2(F_o^2) + (0.0258P)^2 + 0.6993P]$ where $P = (F_o^2 + 2F_c^2)/3$
$(\Delta/\sigma)_{max}$ = 0.002
$\Delta\rho_{max}$ = 0.70 e Å^{-3}
$\Delta\rho_{min}$ = −0.58 e Å^{-3}

Special details

Geometry. All esds (except the esd in the dihedral angle between two l.s. planes) are estimated using the full covariance matrix. The cell esds are taken into account individually in the estimation of esds in distances, angles and torsion angles; correlations between esds in cell parameters are only used when they are defined by crystal symmetry. An approximate (isotropic) treatment of cell esds is used for estimating esds involving l.s. planes.

Fractional atomic coordinates and isotropic or equivalent isotropic displacement parameters (Å²)

	x	*y*	*z*	U_{iso}*/U_{eq}
Fe1	0.47180 (2)	0.37521 (2)	0.81519 (2)	0.01202 (3)
Cl1	0.27817 (3)	0.32101 (2)	0.70046 (2)	0.01732 (5)
Cl2	0.66305 (3)	0.43097 (2)	0.92874 (2)	0.01876 (5)
Cl3	0.52630 (4)	0.35899 (2)	0.21489 (2)	0.02871 (6)
O1	0.40718 (10)	0.38361 (4)	0.44329 (7)	0.02515 (16)
H1C	0.455854	0.378135	0.385847	0.038*
N1	0.58062 (10)	0.40542 (4)	0.67522 (7)	0.01620 (15)
H1	0.5277 (17)	0.3869 (7)	0.6179 (12)	0.019*
N2	0.33640 (10)	0.45956 (4)	0.79670 (7)	0.01590 (15)
H2	0.3834 (17)	0.4855 (7)	0.8429 (12)	0.019*
N3	0.36207 (10)	0.34494 (4)	0.95311 (7)	0.01496 (14)
H3	0.4117 (17)	0.3639 (7)	1.0094 (12)	0.018*
N4	0.60971 (10)	0.29159 (4)	0.83285 (7)	0.01582 (15)
H4	0.5637 (17)	0.2639 (7)	0.7871 (11)	0.019*
C1	0.53940 (13)	0.47461 (5)	0.66291 (9)	0.01939 (18)
H1A	0.557193	0.489153	0.587241	0.023*
H1B	0.611401	0.500151	0.716153	0.023*
C2	0.36108 (13)	0.48431 (5)	0.68441 (9)	0.01946 (18)
H2A	0.332969	0.530483	0.679677	0.023*
H2B	0.288599	0.461058	0.628190	0.023*
C3	0.15991 (12)	0.45597 (5)	0.81998 (8)	0.01685 (17)
H3A	0.102435	0.425920	0.765204	0.020*
C4	0.07595 (14)	0.52151 (5)	0.80674 (10)	0.0237 (2)
H4A	0.076085	0.535789	0.729836	0.036*
H4B	0.135678	0.552648	0.855612	0.036*
H4C	−0.037662	0.518041	0.826315	0.036*
C5	0.14494 (12)	0.42890 (5)	0.93590 (8)	0.01754 (17)
H5A	0.031619	0.437079	0.955525	0.021*
H5B	0.220314	0.453395	0.988641	0.021*
C6	0.18158 (11)	0.35740 (5)	0.95346 (8)	0.01603 (17)
H6	0.123673	0.333249	0.890369	0.019*
C7	0.11429 (14)	0.33419 (6)	1.06051 (9)	0.0239 (2)
H7A	−0.003351	0.344022	1.058253	0.036*
H7B	0.172703	0.355944	1.123865	0.036*
H7C	0.130490	0.287752	1.067843	0.036*
C8	0.40632 (12)	0.27600 (5)	0.96661 (9)	0.01822 (17)
H8A	0.335978	0.249714	0.913538	0.022*
H8B	0.388881	0.261616	1.042426	0.022*
C9	0.58568 (12)	0.26783 (5)	0.94559 (8)	0.01813 (18)

H9A	0.656282	0.292329	1.001177	0.022*
H9B	0.616859	0.222006	0.951977	0.022*
C10	0.78611 (12)	0.29646 (5)	0.80966 (8)	0.01750 (17)
H10	0.840678	0.328751	0.861602	0.021*
C11	0.87818 (14)	0.23277 (5)	0.82714 (11)	0.0256 (2)
H11A	0.820901	0.199402	0.781780	0.038*
H11B	0.882138	0.220565	0.905291	0.038*
H11C	0.990414	0.237568	0.805522	0.038*
C12	0.79645 (13)	0.32071 (5)	0.69159 (9)	0.01947 (18)
H12A	0.718888	0.295318	0.641738	0.023*
H12B	0.908597	0.311878	0.670309	0.023*
C13	0.75944 (12)	0.39183 (5)	0.67087 (9)	0.01846 (18)
H13	0.821325	0.416959	0.731130	0.022*
C14	0.82060 (15)	0.41270 (6)	0.56061 (10)	0.0272 (2)
H14A	0.758797	0.389821	0.499875	0.041*
H14B	0.937854	0.402626	0.560510	0.041*
H14C	0.804288	0.458995	0.550918	0.041*
C15	0.23468 (15)	0.38140 (6)	0.41595 (10)	0.0275 (2)
H15A	0.211506	0.360725	0.343752	0.041*
H15B	0.190455	0.425126	0.412864	0.041*
H15C	0.182924	0.356809	0.472335	0.041*

Atomic displacement parameters (Å^2)

	U^{11}	U^{22}	U^{33}	U^{12}	U^{13}	U^{23}
Fe1	0.01143 (6)	0.01141 (6)	0.01307 (6)	−0.00026 (4)	0.00023 (4)	0.00017 (4)
Cl1	0.01816 (10)	0.01672 (10)	0.01704 (10)	−0.00156 (8)	0.00141 (8)	−0.00360 (8)
Cl2	0.01866 (10)	0.01754 (10)	0.01942 (11)	−0.00260 (8)	−0.00196 (8)	−0.00258 (8)
Cl3	0.02918 (13)	0.03443 (15)	0.02208 (12)	0.00209 (11)	−0.00018 (10)	−0.00469 (10)
O1	0.0250 (4)	0.0287 (4)	0.0214 (4)	−0.0019 (3)	−0.0001 (3)	0.0001 (3)
N1	0.0143 (3)	0.0153 (4)	0.0189 (4)	−0.0012 (3)	0.0008 (3)	−0.0002 (3)
N2	0.0150 (3)	0.0161 (4)	0.0163 (4)	−0.0003 (3)	−0.0003 (3)	−0.0003 (3)
N3	0.0143 (3)	0.0143 (3)	0.0162 (4)	−0.0002 (3)	0.0007 (3)	−0.0007 (3)
N4	0.0136 (3)	0.0166 (4)	0.0170 (4)	−0.0001 (3)	−0.0002 (3)	0.0016 (3)
C1	0.0202 (4)	0.0163 (4)	0.0219 (5)	−0.0007 (3)	0.0029 (4)	0.0049 (3)
C2	0.0199 (4)	0.0175 (4)	0.0209 (4)	0.0026 (3)	0.0014 (3)	0.0045 (3)
C3	0.0138 (4)	0.0170 (4)	0.0194 (4)	0.0022 (3)	−0.0002 (3)	−0.0013 (3)
C4	0.0236 (5)	0.0202 (5)	0.0271 (5)	0.0073 (4)	0.0000 (4)	−0.0005 (4)
C5	0.0163 (4)	0.0175 (4)	0.0191 (4)	0.0016 (3)	0.0029 (3)	−0.0026 (3)
C6	0.0135 (4)	0.0176 (4)	0.0171 (4)	−0.0010 (3)	0.0023 (3)	−0.0011 (3)
C7	0.0216 (5)	0.0281 (5)	0.0229 (5)	−0.0001 (4)	0.0073 (4)	0.0035 (4)
C8	0.0199 (4)	0.0151 (4)	0.0200 (4)	0.0006 (3)	0.0036 (3)	0.0034 (3)
C9	0.0190 (4)	0.0167 (4)	0.0185 (4)	0.0027 (3)	0.0007 (3)	0.0041 (3)
C10	0.0130 (4)	0.0179 (4)	0.0214 (4)	0.0012 (3)	0.0004 (3)	0.0003 (3)
C11	0.0182 (5)	0.0206 (5)	0.0375 (6)	0.0046 (4)	−0.0007 (4)	0.0013 (4)
C12	0.0167 (4)	0.0208 (5)	0.0212 (5)	0.0020 (3)	0.0035 (3)	−0.0014 (4)
C13	0.0146 (4)	0.0207 (4)	0.0204 (4)	−0.0018 (3)	0.0030 (3)	0.0008 (4)
C14	0.0254 (5)	0.0312 (6)	0.0263 (5)	−0.0006 (4)	0.0102 (4)	0.0049 (4)

C15	0.0257 (5)	0.0294 (6)	0.0271 (5)	0.0009 (4)	−0.0001 (4)	0.0010 (4)

Geometric parameters (Å, º)

Fe1—N3	2.0654 (8)	C5—C6	1.5317 (14)
Fe1—N4	2.0761 (8)	C5—H5A	0.9900
Fe1—N2	2.0787 (9)	C5—H5B	0.9900
Fe1—N1	2.0826 (9)	C6—C7	1.5327 (14)
Fe1—Cl2	2.3047 (3)	C6—H6	1.0000
Fe1—Cl1	2.3084 (3)	C7—H7A	0.9800
O1—C15	1.4189 (14)	C7—H7B	0.9800
O1—H1C	0.8400	C7—H7C	0.9800
N1—C1	1.4858 (13)	C8—C9	1.5176 (14)
N1—C13	1.4924 (13)	C8—H8A	0.9900
N1—H1	0.876 (14)	C8—H8B	0.9900
N2—C2	1.4875 (13)	C9—H9A	0.9900
N2—C3	1.4941 (13)	C9—H9B	0.9900
N2—H2	0.847 (14)	C10—C12	1.5291 (15)
N3—C8	1.4875 (13)	C10—C11	1.5313 (15)
N3—C6	1.4965 (12)	C10—H10	1.0000
N3—H3	0.860 (14)	C11—H11A	0.9800
N4—C9	1.4844 (13)	C11—H11B	0.9800
N4—C10	1.4947 (12)	C11—H11C	0.9800
N4—H4	0.864 (14)	C12—C13	1.5295 (15)
C1—C2	1.5148 (15)	C12—H12A	0.9900
C1—H1A	0.9900	C12—H12B	0.9900
C1—H1B	0.9900	C13—C14	1.5320 (15)
C2—H2A	0.9900	C13—H13	1.0000
C2—H2B	0.9900	C14—H14A	0.9800
C3—C4	1.5306 (14)	C14—H14B	0.9800
C3—C5	1.5309 (14)	C14—H14C	0.9800
C3—H3A	1.0000	C15—H15A	0.9800
C4—H4A	0.9800	C15—H15B	0.9800
C4—H4B	0.9800	C15—H15C	0.9800
C4—H4C	0.9800		
N3—Fe1—N4	85.96 (3)	C3—C5—H5A	108.0
N3—Fe1—N2	94.69 (3)	C6—C5—H5A	108.0
N4—Fe1—N2	179.23 (3)	C3—C5—H5B	108.0
N3—Fe1—N1	179.48 (3)	C6—C5—H5B	108.0
N4—Fe1—N1	94.13 (3)	H5A—C5—H5B	107.3
N2—Fe1—N1	85.23 (3)	N3—C6—C5	110.41 (8)
N3—Fe1—Cl2	89.34 (2)	N3—C6—C7	111.94 (8)
N4—Fe1—Cl2	91.66 (3)	C5—C6—C7	110.19 (8)
N2—Fe1—Cl2	87.92 (3)	N3—C6—H6	108.1
N1—Fe1—Cl2	91.17 (3)	C5—C6—H6	108.1
N3—Fe1—Cl1	90.97 (2)	C7—C6—H6	108.1
N4—Fe1—Cl1	89.30 (3)	C6—C7—H7A	109.5

N2—Fe1—Cl1	91.11 (3)	C6—C7—H7B	109.5
N1—Fe1—Cl1	88.53 (2)	H7A—C7—H7B	109.5
Cl2—Fe1—Cl1	179.012 (11)	C6—C7—H7C	109.5
C15—O1—H1C	109.5	H7A—C7—H7C	109.5
C1—N1—C13	113.23 (8)	H7B—C7—H7C	109.5
C1—N1—Fe1	105.46 (6)	N3—C8—C9	108.56 (8)
C13—N1—Fe1	117.38 (6)	N3—C8—H8A	110.0
C1—N1—H1	104.9 (9)	C9—C8—H8A	110.0
C13—N1—H1	107.7 (9)	N3—C8—H8B	110.0
Fe1—N1—H1	107.4 (9)	C9—C8—H8B	110.0
C2—N2—C3	113.63 (8)	H8A—C8—H8B	108.4
C2—N2—Fe1	106.20 (6)	N4—C9—C8	108.96 (8)
C3—N2—Fe1	116.71 (6)	N4—C9—H9A	109.9
C2—N2—H2	107.2 (10)	C8—C9—H9A	109.9
C3—N2—H2	107.2 (9)	N4—C9—H9B	109.9
Fe1—N2—H2	105.3 (9)	C8—C9—H9B	109.9
C8—N3—C6	113.39 (8)	H9A—C9—H9B	108.3
C8—N3—Fe1	105.43 (6)	N4—C10—C12	109.40 (8)
C6—N3—Fe1	116.51 (6)	N4—C10—C11	112.60 (8)
C8—N3—H3	105.4 (9)	C12—C10—C11	110.48 (9)
C6—N3—H3	108.2 (9)	N4—C10—H10	108.1
Fe1—N3—H3	107.2 (9)	C12—C10—H10	108.1
C9—N4—C10	113.80 (8)	C11—C10—H10	108.1
C9—N4—Fe1	105.13 (6)	C10—C11—H11A	109.5
C10—N4—Fe1	116.50 (6)	C10—C11—H11B	109.5
C9—N4—H4	106.5 (9)	H11A—C11—H11B	109.5
C10—N4—H4	107.3 (9)	C10—C11—H11C	109.5
Fe1—N4—H4	107.1 (9)	H11A—C11—H11C	109.5
N1—C1—C2	108.96 (8)	H11B—C11—H11C	109.5
N1—C1—H1A	109.9	C10—C12—C13	116.63 (8)
C2—C1—H1A	109.9	C10—C12—H12A	108.1
N1—C1—H1B	109.9	C13—C12—H12A	108.1
C2—C1—H1B	109.9	C10—C12—H12B	108.1
H1A—C1—H1B	108.3	C13—C12—H12B	108.1
N2—C2—C1	108.71 (8)	H12A—C12—H12B	107.3
N2—C2—H2A	109.9	N1—C13—C12	110.98 (8)
C1—C2—H2A	109.9	N1—C13—C14	111.81 (9)
N2—C2—H2B	109.9	C12—C13—C14	110.13 (9)
C1—C2—H2B	109.9	N1—C13—H13	107.9
H2A—C2—H2B	108.3	C12—C13—H13	107.9
N2—C3—C4	111.45 (8)	C14—C13—H13	107.9
N2—C3—C5	110.38 (8)	C13—C14—H14A	109.5
C4—C3—C5	110.76 (8)	C13—C14—H14B	109.5
N2—C3—H3A	108.0	H14A—C14—H14B	109.5
C4—C3—H3A	108.0	C13—C14—H14C	109.5
C5—C3—H3A	108.0	H14A—C14—H14C	109.5
C3—C4—H4A	109.5	H14B—C14—H14C	109.5
C3—C4—H4B	109.5	O1—C15—H15A	109.5

H4A—C4—H4B	109.5	O1—C15—H15B	109.5
C3—C4—H4C	109.5	H15A—C15—H15B	109.5
H4A—C4—H4C	109.5	O1—C15—H15C	109.5
H4B—C4—H4C	109.5	H15A—C15—H15C	109.5
C3—C5—C6	117.15 (8)	H15B—C15—H15C	109.5

C13—N1—C1—C2	−172.15 (8)	C6—N3—C8—C9	170.51 (8)
Fe1—N1—C1—C2	−42.52 (9)	Fe1—N3—C8—C9	41.92 (9)
C3—N2—C2—C1	−169.94 (8)	C10—N4—C9—C8	170.11 (8)
Fe1—N2—C2—C1	−40.29 (9)	Fe1—N4—C9—C8	41.47 (9)
N1—C1—C2—N2	57.18 (11)	N3—C8—C9—N4	−57.87 (10)
C2—N2—C3—C4	−57.59 (11)	C9—N4—C10—C12	179.51 (8)
Fe1—N2—C3—C4	178.28 (7)	Fe1—N4—C10—C12	−57.89 (9)
C2—N2—C3—C5	178.90 (8)	C9—N4—C10—C11	56.26 (11)
Fe1—N2—C3—C5	54.76 (9)	Fe1—N4—C10—C11	178.86 (7)
N2—C3—C5—C6	−71.58 (11)	N4—C10—C12—C13	74.04 (11)
C4—C3—C5—C6	164.50 (9)	C11—C10—C12—C13	−161.46 (9)
C8—N3—C6—C5	−178.37 (8)	C1—N1—C13—C12	176.24 (8)
Fe1—N3—C6—C5	−55.71 (9)	Fe1—N1—C13—C12	52.95 (10)
C8—N3—C6—C7	58.47 (11)	C1—N1—C13—C14	−60.37 (11)
Fe1—N3—C6—C7	−178.86 (7)	Fe1—N1—C13—C14	176.34 (7)
C3—C5—C6—N3	72.14 (11)	C10—C12—C13—N1	−71.47 (11)
C3—C5—C6—C7	−163.68 (9)	C10—C12—C13—C14	164.17 (9)

Hydrogen-bond geometry (Å, º)

D—H···*A*	*D*—H	H···*A*	*D*···*A*	*D*—H···*A*
O1—H1*C*···Cl3	0.84	2.24	3.0607 (9)	167
N1—H1···O1	0.876 (14)	2.258 (15)	3.0723 (12)	154.5 (12)
N3—H3···Cl3^{i}	0.860 (14)	2.588 (14)	3.3518 (9)	148.5 (12)
N4—H4···Cl3^{ii}	0.864 (14)	2.716 (14)	3.4925 (9)	150.2 (12)

Symmetry codes: (i) *x*, *y*, *z*+1; (ii) *x*, −*y*+1/2, *z*+1/2.

cis-Dichlorido[(5*SR*,7*RS*,12*SR*,14*RS*)-5,7,12,14-tetramethyl-1,4,8,11-tetraazacyclotetradecane]iron(III) chloride (2)

Crystal data

$[Fe(C_{14}H_{32}N_4)Cl_2]Cl$
M_r = 418.63
Orthorhombic, *Pbcn*
a = 9.2912 (12) Å
b = 11.9579 (19) Å
c = 17.267 (3) Å
V = 1918.4 (5) Å^3
Z = 4
F(000) = 884
D_x = 1.449 Mg m^{-3}
Cu *Kα* radiation, *λ* = 1.54178 Å
Cell parameters from 2788 reflections
θ = 6.6–78.2°
μ = 10.15 mm^{-1}
T = 150 K
Block, yellow
0.12 × 0.08 × 0.05 mm

Data collection

Bruker AXS D8 Quest diffractometer with PhotonII charge-integrating pixel array detector (CPAD)
Radiation source: I-mu-S microsource X-ray tube
Laterally graded multilayer (Goebel) mirror monochromator
Detector resolution: 7.4074 pixels mm^{-1}
ω and phi scans

Absorption correction: multi-scan (SADABS; Krause *et al.*, 2015)
T_{min} = 0.526, T_{max} = 0.754
14150 measured reflections
2055 independent reflections
1324 reflections with $I > 2\sigma(I)$
R_{int} = 0.082
θ_{max} = 79.6°, θ_{min} = 6.6°
$h = -11 \rightarrow 9$
$k = -14 \rightarrow 15$
$l = -21 \rightarrow 15$

Refinement

Refinement on F^2
Least-squares matrix: full
$R[F^2 > 2\sigma(F^2)]$ = 0.066
$wR(F^2)$ = 0.196
S = 1.08
2055 reflections
196 parameters
273 restraints
Primary atom site location: structure-invariant direct methods

Secondary atom site location: difference Fourier map
Hydrogen site location: inferred from neighbouring sites
H-atom parameters constrained
$w = 1/[\sigma^2(F_o^2) + (0.0894P)^2 + 2.1112P]$ where $P = (F_o^2 + 2F_c^2)/3$
$(\Delta/\sigma)_{max}$ < 0.001
$\Delta\rho_{max}$ = 0.58 e Å^{-3}
$\Delta\rho_{min}$ = −0.95 e Å^{-3}

Special details

Geometry. All esds (except the esd in the dihedral angle between two l.s. planes) are estimated using the full covariance matrix. The cell esds are taken into account individually in the estimation of esds in distances, angles and torsion angles; correlations between esds in cell parameters are only used when they are defined by crystal symmetry. An approximate (isotropic) treatment of cell esds is used for estimating esds involving l.s. planes.

Refinement. The entire cationic moiety, excluding the central Fe ion, is disordered about a pseudo-mirror plane through the metal center. The two moieties were restrained to have similar anisotropic displacement parameters (SIMU command) and similar 1,2 and 1,3 bond distances (SAME command). Additionally, the distances between C1 and N2, and C1B and N2B were restrained to be similar (SADI command). The two moieties refined to a roughly 0.944 (3) to 0.056 (3) occupancy ratio. Interestingly, analysis of H-bonds revealed extensive hydrogen bonding between both orientations and the chloride counteranion. This high level of hydrogen bonding in the disordered position may facilitate the occupancy of the second position.

Fractional atomic coordinates and isotropic or equivalent isotropic displacement parameters (Å^2)

	x	y	z	U_{iso}*/U_{eq}	Occ. (<1)
Cl1	0.06475 (16)	0.14880 (11)	0.33931 (8)	0.0527 (4)	0.944 (3)
N1	0.0818 (4)	−0.1126 (4)	0.3317 (2)	0.0400 (9)	0.944 (3)
H1	0.056778	−0.187227	0.309366	0.048*	0.944 (3)
N2	−0.2090 (4)	−0.0128 (3)	0.3004 (3)	0.0411 (10)	0.944 (3)
H2	−0.265622	0.055663	0.287131	0.049*	0.944 (3)
C1	0.2829 (6)	−0.1056 (5)	0.2418 (3)	0.0476 (15)	0.944 (3)
H1A	0.254084	−0.178590	0.219657	0.057*	0.944 (3)
H1AB	0.388537	−0.097899	0.236565	0.057*	0.944 (3)
C2	0.2414 (5)	−0.1003 (5)	0.3253 (3)	0.0471 (12)	0.944 (3)
H2A	0.271799	−0.027846	0.347721	0.056*	0.944 (3)
H2AB	0.289690	−0.161001	0.354366	0.056*	0.944 (3)

C3	0.0315 (6)	−0.1130 (5)	0.4128 (3)	0.0452 (12)	0.944 (3)
H3	0.061690	−0.040932	0.437252	0.054*	0.944 (3)
C4	0.0983 (7)	−0.2084 (5)	0.4591 (3)	0.0595 (16)	0.944 (3)
H4A	0.073991	−0.279922	0.434715	0.089*	0.944 (3)
H4B	0.060796	−0.207092	0.512146	0.089*	0.944 (3)
H4C	0.203153	−0.199423	0.460242	0.089*	0.944 (3)
C5	−0.1317 (6)	−0.1208 (5)	0.4178 (3)	0.0476 (12)	0.944 (3)
H5A	−0.158073	−0.131177	0.472879	0.057*	0.944 (3)
H5AB	−0.162259	−0.189054	0.389749	0.057*	0.944 (3)
C6	−0.2191 (6)	−0.0219 (5)	0.3860 (3)	0.0489 (13)	0.944 (3)
H6	−0.175674	0.047726	0.408015	0.059*	0.944 (3)
C7	−0.3738 (7)	−0.0272 (5)	0.4148 (4)	0.0647 (18)	0.944 (3)
H7A	−0.430007	0.032673	0.390680	0.097*	0.944 (3)
H7B	−0.375245	−0.018051	0.471227	0.097*	0.944 (3)
H7C	−0.415638	−0.099831	0.401155	0.097*	0.944 (3)
Cl1B	−0.063 (2)	0.1467 (16)	0.3395 (14)	0.050 (6)	0.056 (3)
N1B	−0.073 (3)	−0.115 (2)	0.331 (2)	0.044 (2)	0.056 (3)
H1B	−0.045655	−0.188536	0.307266	0.053*	0.056 (3)
N2B	0.216 (3)	−0.009 (3)	0.301 (2)	0.045 (3)	0.056 (3)
H2B	0.276232	0.056964	0.286463	0.054*	0.056 (3)
C1B	−0.274 (6)	−0.109 (6)	0.241 (4)	0.042 (5)	0.056 (3)
H1B1	−0.379699	−0.109911	0.236360	0.051*	0.056 (3)
H1B2	−0.235446	−0.177516	0.216807	0.051*	0.056 (3)
C2B	−0.233 (4)	−0.107 (8)	0.325 (3)	0.045 (3)	0.056 (3)
H2BA	−0.266504	−0.036365	0.348968	0.053*	0.056 (3)
H2BB	−0.278760	−0.170198	0.352068	0.053*	0.056 (3)
C3B	−0.022 (4)	−0.119 (4)	0.412 (2)	0.045 (3)	0.056 (3)
H3B	−0.054828	−0.049100	0.438483	0.054*	0.056 (3)
C4B	−0.085 (6)	−0.219 (6)	0.456 (3)	0.051 (6)	0.056 (3)
H4BA	−0.180181	−0.236572	0.434966	0.077*	0.056 (3)
H4BB	−0.093223	−0.199981	0.510851	0.077*	0.056 (3)
H4BC	−0.021138	−0.283390	0.449623	0.077*	0.056 (3)
C5B	0.141 (4)	−0.124 (4)	0.416 (3)	0.045 (3)	0.056 (3)
H5BA	0.173758	−0.189970	0.386439	0.054*	0.056 (3)
H5BB	0.168807	−0.136472	0.470953	0.054*	0.056 (3)
C6B	0.225 (4)	−0.022 (3)	0.387 (2)	0.044 (3)	0.056 (3)
H6B	0.178104	0.045868	0.409690	0.052*	0.056 (3)
C7B	0.379 (5)	−0.024 (5)	0.417 (4)	0.038 (10)	0.056 (3)
H7BA	0.429323	0.043945	0.400233	0.057*	0.056 (3)
H7BB	0.428749	−0.089744	0.395976	0.057*	0.056 (3)
H7BC	0.377971	−0.027770	0.473444	0.057*	0.056 (3)
Fe1	0.000000	0.01505 (8)	0.250000	0.0378 (4)	
Cl2	0.500000	0.14810 (14)	0.250000	0.0466 (5)	

Atomic displacement parameters (Å²)

	U^{11}	U^{22}	U^{33}	U^{12}	U^{13}	U^{23}
Cl1	0.0588 (8)	0.0373 (7)	0.0618 (9)	−0.0080 (6)	0.0109 (7)	−0.0082 (6)

N1	0.037 (2)	0.033 (2)	0.049 (2)	0.0059 (15)	−0.0023 (17)	−0.0005 (17)
N2	0.037 (2)	0.033 (2)	0.053 (2)	0.0053 (16)	0.0089 (18)	0.0072 (18)
C1	0.038 (3)	0.039 (3)	0.065 (4)	0.006 (2)	0.004 (2)	−0.003 (3)
C2	0.038 (2)	0.041 (3)	0.062 (3)	0.004 (2)	−0.004 (2)	−0.002 (2)
C3	0.050 (3)	0.040 (3)	0.046 (3)	0.008 (2)	0.001 (2)	−0.002 (2)
C4	0.075 (4)	0.053 (4)	0.051 (3)	0.017 (3)	−0.003 (3)	0.006 (3)
C5	0.049 (3)	0.044 (3)	0.049 (3)	0.005 (2)	0.007 (2)	0.008 (2)
C6	0.047 (3)	0.049 (3)	0.050 (3)	0.006 (2)	0.016 (2)	0.011 (2)
C7	0.056 (3)	0.065 (4)	0.074 (4)	0.012 (3)	0.025 (3)	0.017 (3)
Cl1B	0.039 (9)	0.033 (9)	0.079 (13)	0.021 (7)	−0.030 (9)	−0.038 (9)
N1B	0.044 (4)	0.039 (4)	0.049 (4)	0.005 (4)	0.007 (4)	0.005 (4)
N2B	0.039 (6)	0.037 (6)	0.058 (6)	0.004 (5)	−0.004 (5)	0.000 (6)
C1B	0.039 (8)	0.035 (8)	0.053 (8)	0.008 (8)	0.009 (8)	0.006 (8)
C2B	0.043 (5)	0.039 (5)	0.051 (5)	0.005 (5)	0.010 (5)	0.007 (5)
C3B	0.046 (5)	0.039 (5)	0.049 (5)	0.006 (5)	0.002 (5)	0.002 (5)
C4B	0.058 (10)	0.046 (10)	0.050 (10)	0.007 (10)	0.001 (10)	0.007 (10)
C5B	0.044 (5)	0.039 (5)	0.052 (5)	0.007 (5)	−0.002 (5)	0.001 (5)
C6B	0.039 (6)	0.037 (6)	0.055 (6)	0.004 (6)	−0.005 (6)	0.000 (6)
C7B	0.037 (19)	0.015 (18)	0.06 (2)	−0.013 (17)	−0.018 (19)	0.004 (18)
Fe1	0.0342 (5)	0.0301 (6)	0.0492 (7)	0.000	0.0037 (4)	0.000
Cl2	0.0444 (9)	0.0317 (9)	0.0638 (12)	0.000	0.0015 (8)	0.000

Geometric parameters (Å, º)

Cl1—Fe1	2.3018 (15)	Cl1B—Fe1	2.283 (18)
N1—C3	1.476 (6)	N1B—C3B	1.475 (12)
N1—C2	1.494 (6)	N1B—C2B	1.494 (12)
N1—Fe1	2.213 (4)	N1B—Fe1	2.20 (3)
N1—H1	1.0000	N1B—H1B	1.0000
N2—C6	1.485 (7)	N2B—C6B	1.484 (13)
N2—C1^{i}	1.495 (7)	N2B—C1B^{i}	1.50 (2)
N2—Fe1	2.154 (4)	N2B—Fe1	2.21 (3)
N2—H2	1.0000	N2B—H2B	1.0000
C1—C2	1.493 (7)	C1B—C2B	1.495 (13)
C1—H1A	0.9900	C1B—H1B1	0.9900
C1—H1AB	0.9900	C1B—H1B2	0.9900
C2—H2A	0.9900	C2B—H2BA	0.9900
C2—H2AB	0.9900	C2B—H2BB	0.9900
C3—C5	1.522 (7)	C3B—C5B	1.524 (13)
C3—C4	1.525 (7)	C3B—C4B	1.526 (13)
C3—H3	1.0000	C3B—H3B	1.0000
C4—H4A	0.9800	C4B—H4BA	0.9800
C4—H4B	0.9800	C4B—H4BB	0.9800
C4—H4C	0.9800	C4B—H4BC	0.9800
C5—C6	1.537 (7)	C5B—C6B	1.537 (13)
C5—H5A	0.9900	C5B—H5BA	0.9900
C5—H5AB	0.9900	C5B—H5BB	0.9900
C6—C7	1.522 (8)	C6B—C7B	1.522 (13)

C6—H6	1.0000	C6B—H6B	1.0000
C7—H7A	0.9800	C7B—H7BA	0.9800
C7—H7B	0.9800	C7B—H7BB	0.9800
C7—H7C	0.9800	C7B—H7BC	0.9800

C3—N1—C2	112.6 (4)	N2B^{i}—C1B—H1B2	109.3
C3—N1—Fe1	119.9 (3)	H1B1—C1B—H1B2	107.9
C2—N1—Fe1	103.0 (3)	N1B—C2B—C1B	108.7 (16)
C3—N1—H1	106.8	N1B—C2B—H2BA	110.0
C2—N1—H1	106.8	C1B—C2B—H2BA	110.0
Fe1—N1—H1	106.8	N1B—C2B—H2BB	110.0
C6—N2—C1^{i}	113.8 (4)	C1B—C2B—H2BB	110.0
C6—N2—Fe1	118.1 (3)	H2BA—C2B—H2BB	108.3
C1^{i}—N2—Fe1	109.4 (3)	N1B—C3B—C5B	111.4 (16)
C6—N2—H2	104.7	N1B—C3B—C4B	111.8 (16)
C1^{i}—N2—H2	104.7	C5B—C3B—C4B	109.1 (16)
Fe1—N2—H2	104.7	N1B—C3B—H3B	108.1
C2—C1—N2^{i}	108.7 (4)	C5B—C3B—H3B	108.1
C2—C1—H1A	109.9	C4B—C3B—H3B	108.1
N2^{i}—C1—H1A	109.9	C3B—C4B—H4BA	109.5
C2—C1—H1AB	109.9	C3B—C4B—H4BB	109.5
N2^{i}—C1—H1AB	109.9	H4BA—C4B—H4BB	109.5
H1A—C1—H1AB	108.3	C3B—C4B—H4BC	109.5
C1—C2—N1	108.9 (4)	H4BA—C4B—H4BC	109.5
C1—C2—H2A	109.9	H4BB—C4B—H4BC	109.5
N1—C2—H2A	109.9	C3B—C5B—C6B	117.3 (17)
C1—C2—H2AB	109.9	C3B—C5B—H5BA	108.0
N1—C2—H2AB	109.9	C6B—C5B—H5BA	108.0
H2A—C2—H2AB	108.3	C3B—C5B—H5BB	108.0
N1—C3—C5	111.7 (4)	C6B—C5B—H5BB	108.0
N1—C3—C4	111.8 (4)	H5BA—C5B—H5BB	107.2
C5—C3—C4	109.3 (5)	N2B—C6B—C7B	113.2 (17)
N1—C3—H3	108.0	N2B—C6B—C5B	112.5 (16)
C5—C3—H3	108.0	C7B—C6B—C5B	110.3 (16)
C4—C3—H3	108.0	N2B—C6B—H6B	106.8
C3—C4—H4A	109.5	C7B—C6B—H6B	106.8
C3—C4—H4B	109.5	C5B—C6B—H6B	106.8
H4A—C4—H4B	109.5	C6B—C7B—H7BA	109.5
C3—C4—H4C	109.5	C6B—C7B—H7BB	109.5
H4A—C4—H4C	109.5	H7BA—C7B—H7BB	109.5
H4B—C4—H4C	109.5	C6B—C7B—H7BC	109.5
C3—C5—C6	117.3 (5)	H7BA—C7B—H7BC	109.5
C3—C5—H5A	108.0	H7BB—C7B—H7BC	109.5
C6—C5—H5A	108.0	N2—Fe1—N2^{i}	162.2 (2)
C3—C5—H5AB	108.0	N2—Fe1—N1B^{i}	115.1 (9)
C6—C5—H5AB	108.0	N2^{i}—Fe1—N1B^{i}	49.9 (9)
H5A—C5—H5AB	107.2	N2—Fe1—N2B^{i}	47.4 (10)
N2—C6—C7	112.8 (5)	N2^{i}—Fe1—N2B^{i}	129.5 (9)

N2—C6—C5	112.2 (4)	N1B—Fe1—N2B	86.1 (11)
C7—C6—C5	110.5 (4)	N1B^{i}—Fe1—N2B	83.3 (15)
N2—C6—H6	107.0	N2B^{i}—Fe1—N2B	165 (2)
C7—C6—H6	107.0	N2—Fe1—N1	86.85 (15)
C5—C6—H6	107.0	N2^{i}—Fe1—N1	80.87 (16)
C6—C7—H7A	109.5	N2—Fe1—N1^{i}	80.87 (16)
C6—C7—H7B	109.5	N2^{i}—Fe1—N1^{i}	86.85 (15)
H7A—C7—H7B	109.5	N1—Fe1—N1^{i}	92.8 (2)
C6—C7—H7C	109.5	N1B—Fe1—Cl1B	88.8 (10)
H7A—C7—H7C	109.5	N1B^{i}—Fe1—Cl1B	176.1 (10)
H7B—C7—H7C	109.5	N2B^{i}—Fe1—Cl1B	97.3 (10)
C3B—N1B—C2B	112.8 (16)	N2B—Fe1—Cl1B	92.9 (10)
C3B—N1B—Fe1	121.7 (17)	N2—Fe1—Cl1B^{i}	127.7 (5)
C2B—N1B—Fe1	102 (3)	N2^{i}—Fe1—Cl1B^{i}	66.5 (6)
C3B—N1B—H1B	106.4	N1—Fe1—Cl1B^{i}	145.0 (5)
C2B—N1B—H1B	106.4	N1^{i}—Fe1—Cl1B^{i}	97.6 (6)
Fe1—N1B—H1B	106.4	N2—Fe1—Cl1	94.16 (12)
C6B—N2B—C1B^{i}	113 (4)	N2^{i}—Fe1—Cl1	98.20 (12)
C6B—N2B—Fe1	117.5 (16)	N1—Fe1—Cl1	87.83 (12)
C1B^{i}—N2B—Fe1	103 (3)	N1^{i}—Fe1—Cl1	174.94 (11)
C6B—N2B—H2B	107.6	N2—Fe1—Cl1^{i}	98.20 (12)
C1B^{i}—N2B—H2B	107.6	N2^{i}—Fe1—Cl1^{i}	94.16 (12)
Fe1—N2B—H2B	107.6	N1—Fe1—Cl1^{i}	174.94 (11)
C2B—C1B—H1B1	109.3	N1^{i}—Fe1—Cl1^{i}	87.83 (12)
N2B^{i}—C1B—H1B1	109.3	Cl1—Fe1—Cl1^{i}	91.97 (8)
C2B—C1B—H1B2	109.3		

N2^{i}—C1—C2—N1	59.8 (6)	C3B—N1B—C2B—C1B	−178 (5)
C3—N1—C2—C1	177.6 (4)	Fe1—N1B—C2B—C1B	50 (6)
Fe1—N1—C2—C1	−51.8 (5)	N2B^{i}—C1B—C2B—N1B	−64 (8)
C2—N1—C3—C5	177.7 (4)	C2B—N1B—C3B—C5B	−178 (5)
Fe1—N1—C3—C5	56.2 (5)	Fe1—N1B—C3B—C5B	−56 (3)
C2—N1—C3—C4	−59.5 (6)	C2B—N1B—C3B—C4B	60 (5)
Fe1—N1—C3—C4	179.0 (4)	Fe1—N1B—C3B—C4B	−178 (3)
N1—C3—C5—C6	−65.4 (6)	N1B—C3B—C5B—C6B	65 (3)
C4—C3—C5—C6	170.4 (5)	C4B—C3B—C5B—C6B	−171 (3)
C1^{i}—N2—C6—C7	−56.8 (6)	C1B^{i}—N2B—C6B—C7B	67 (5)
Fe1—N2—C6—C7	173.0 (4)	Fe1—N2B—C6B—C7B	−173 (3)
C1^{i}—N2—C6—C5	68.8 (6)	C1B^{i}—N2B—C6B—C5B	−59 (4)
Fe1—N2—C6—C5	−61.4 (5)	Fe1—N2B—C6B—C5B	61 (3)
C3—C5—C6—N2	68.8 (7)	C3B—C5B—C6B—N2B	−70 (3)
C3—C5—C6—C7	−164.3 (5)	C3B—C5B—C6B—C7B	163 (3)

Symmetry code: (i) $-x$, y, $-z+1/2$.

Hydrogen-bond geometry (Å, º)

D—H···*A*	*D*—H	H···*A*	*D*···*A*	*D*—H···*A*
N1—H1···Cl2^{ii}	1.00	2.28	3.280 (5)	176

N2—H2···Cl2^{iii}	1.00	2.52	3.431 (4)	151
N1*B*—H1*B*···Cl2^{ii}	1.00	2.23	3.23 (3)	176
N2*B*—H2*B*···Cl2	1.00	2.43	3.36 (3)	154

Symmetry codes: (ii) $x-1/2$, $y-1/2$, $-z+1/2$; (iii) $x-1$, y, z.